Bull. Chem. Soc. Jpn., **68**, 262—276(1995)

Sequential Electron Transfer Leading to Long-Lived Charge Separated State in a Porphyrin–Oxochlorin–Pyromellitdimide Triad

Atsuhiro Osuka,* Shinji Marumo, Kazuhiro Maruyama, Noboru Mataga,*,† Yoshinori Tanaka,† Seiji Taniguchi,† Tadashi Okada,† Iwao Yamazaki,†† and Yoshinobu Nishimura††

Department of Chemistry, Faculty of Science, Kyoto University, Kyoto 606

†Department of Chemistry, Faculty of Engineering Science, Osaka University, Toyonaka 560

††Department of Chemical Process Engineering, Faculty of Engineering, Hokkaido University, Sapporo 060

(Received July 5, 1994)

The synthesis and excited-state dynamics are described for fixed-distance porphyrin–oxochlorin–pyromellitdimide triads (P–C–Im) and related reference compounds. In zinc-oxochlorin–pyromellitdimide (ZnP–Im), the $^1(ZnC)^*$ is quenched by the attached Im through intramolecular charge separation (CS) in benzene, THF, and DMF, while the $^1(H_2C)^*$ in the corresponding free base is not significantly quenched by the Im even in polar DMF. In the steady-state fluorescence emission spectra, only the emission from the $^1(C)^*$ is commonly observed, indicating an efficient intramolecular singlet–singlet excitation energy transfer from P to C. Of these, the fluorescence intensities of the $^1(H_2C)^*$ in ZnP–H_2C and ZnP–H_2C–Im are significantly reduced in polar DMF solution and this is attributed to the intramolecular CS that gives $(ZnP)^+$–$(H_2C)^-$–Im and $(ZnP)^+$–$(H_2C)^-$, respectively. The $(ZnP)^+$–$(H_2C)^-$–Im ion pair is clearly shown, by picosecond absorption spectroscopy, to be converted into a secondary, longer-lived charge separated state $(ZnP)^+$–H_2C–$(Im)^-$ via charge-shift reaction in competition with wasteful charge recombination to the ground state. The $(ZnP)^+$–H_2C–$(Im)^-$ state is formed in 0.09 quantum yield from ZnP–$^1(H_2C)^*$–Im and has a lifetime of 0.24 μs in DMF.

The photoinduced transfer of an electron across a phospholipid membrane in photosynthesis is one of nature's most remarkable achievements. The pathways followed by the electron is extremely intricate, consisting of a series of electron transfers (ET) between various redox components embedded within a transmembrane protein, the photosynthetic reaction center (RC). In the RC, six tetrapyrrolic subunits and two quinones are positioned at precise distances and orientations to realize a nearly quantitative charge separation (CS) through remarkably efficient sequential ET reactions.[1] The initial ET event in the RC is a photoinduced CS between chlorophyll derivatives, giving an ion pair (IP) state, (special pair, SP)$^+$–(bacteriopheophytin, BPh)$^-$ within ca. 3 ps,[2,3] and a subsequent charge-shift reaction (CSH) from $(BPh)^-$ to the quinone Q_A yields a stable IP state $(SP)^+$–$(Q_A)^-$ in ca. 200 ps, thereby separating charges at ca. 28 Å, and a further CSH to Q_B more stabilizes separated charges, thus precluding charge recombination (CR) to the ground state and the energy thus stored is used to drive subsequent chemical processes.

Over the past 15 years or so, a number of model studies have been undertaken in an attempt to understand the ET processes in the RC, to achieve long-lived charge-separated states, and/or to mimic the ET events in the RC.[4] These systems range from relatively simple porphyrins with a singly attached quinone (dyads) to more elaborate multicomponent assemblies (triads, tetrads, pentads) bearing electron acceptors or electron donors with varying coupling strength and conformational rigidities. Among these, spatially well-defined molecules continue to provide opportunities for systematic studies on factors governing rates of ET reactions including driving forces, distances and orientations, the nature of a bridging group, and solvent properties. Intramolecular ET from the singlet excited state of porphyrin to the attached acceptor produces an ion pair (IP) state in the singlet manifold, $(porphyrin)^+$–$(acceptor)^-$, which is usually too short-lived, especially in polar solvents, to be utilized for other chemical reactions. Therefore triplet-photochemistry derived ET has been often employed as a trigger in a variety of model studies aiming at artificial photosynthesis, since charge recombination in triplet IP states is much slower owing to spin restriction.[5] On

the other hand, recent efforts in artificial photosynthesis have culminated in generation of long-lived charge separated states lasting more than several hundreds of microseconds at room temperature through multistep ET sequences triggered by an ET reaction within the singlet manifold.[4,6] To date, however, the vast majority of models are triads D–P–A and stand on the reaction sequence of Eq. 1, where initial CS between the porphyrin (P) and the acceptor (A) is followed by an hole transfer (HT) to the attached donor (D), giving a secondary IP state $(D)^+$–P–$(A)^-$.[6—9] In another strategy, P–(acceptor 1, A_1)–(acceptor 2, A_2) triads were employed, where a secondary CSH reaction from A_1 to A_2 can lead to a long-lived IP state (Eq. 2). Sakata and Mataga first prepared such a triad and revealed a sequential ET-relay in the singlet manifold by the picosecond laser photolysis studies.[10,11] Gust and Moore developed a structurally rigid porphyrin–diquinone moiety and achieved long-lived IP states in its carotenoid-incorporated models.[6] Recently we also made a series of porphyrin–pyromellitdimide–quinone triads and have succeeded in an unambiguous detection of sequential ET-relay that conforms to Eq. 2.[12] However, the reaction sequences of Eqs. 1 and 2 so far attained in artificial models[6—12] differ from the ET-relay within the RC, in that the primary ET is not CS between tetrapyrrole pigments. We are not aware of triads P_1–P_2–A in which a fully charge separated IP state, $(P_1)^+$–P_2–$(A)^-$, is generated via an initial intramolecular CS between the macrocycles P_1 and P_2 followed by a CSH reaction to the electron acceptor A (Eqs. 3 and 4):[13] the ET sequence in Eq. 3 is of course much closer to the reaction mode in the RC.

$$D\text{–}{}^1(P)^*\text{–}A \longrightarrow D\text{–}(P)^+\text{–}(A)^- \longrightarrow (D)^+\text{–}P\text{–}(A)^- \quad (1)$$

$$^1(P)^*\text{–}A_1\text{–}A_2 \longrightarrow (P)^+\text{–}(A_1)^-\text{–}A_2 \longrightarrow (P)^+\text{–}A_1\text{–}(A_2)^- \quad (2)$$

$$^1(P_1)^*\text{–}P_2\text{–}A \longrightarrow (P_1)^+\text{–}(P_2)^-\text{–}A \longrightarrow (P_1)^+\text{–}P_2\text{–}(A)^- \quad (3)$$

$$P_1\text{–}{}^1(P_2)^*\text{–}A \longrightarrow (P_1)^+\text{–}(P_2)^-\text{–}A \longrightarrow (P_1)^+\text{–}P_2\text{–}(A)^- \quad (4)$$

It should be noted here that, for this type of photoinduced CS to occur between similar or identical chromophores, a CT state needs to be stabilized to the energy level lower than the S_1 state by interactions with asymmetric polar environments. As an extreme case of such identical chromophores, we reported solvation-induced symmetry breaking in the singlet excited state of the symmetric bichromophore 9,9′-bianthryl in polar solutions many years ago.[14] For almost complete CS the electronic interactions between the bichromophores must be weak or moderate. If it is too strong, only partial CS can take place due to significant delocalization interactions even in strongly polar solutions as is the case for 9,9′-bianthryl where two anthryls are directly combined.[15] Complete photoinduced CS in strongly polar solution was observed for 1,2-dianthrylethanes with moderately weak inter-chromophore interactions.[16] These fundamental aspects may be common to bichromophoric systems and should be considered in design of photosynthetic models that undergo sequential ET relays according to Eqs. 3 and 4.

Recently, Wasielewski et al. have reported the synthesis and intramolecular ET reactions of a series of fixed-distance, orthogonal, directly attached pyropheophorbide–porphyrin dyads.[17] Zinc complexes either at the both macrocycles or at only the porphyrin core display lowest excited singlet state lifetimes and fluorescence quantum yields that are strongly solvent polarity dependent. Upon laser excitation of a zinc-porphyrin–free base pyropheophorbide dyad in butyronitrile, a distinct IP state with a 43-ps lifetime was observed by the transient absorption measurements. They also reported pyropheophorbide–porphyrin–electron acceptor triads, which upon selective excitation of the pyropheophorbide moiety provide a $(\text{pyropheophorbide})^+$–porphyrin–$(\text{electron acceptor})^-$ IP state in a remarkably high yield by a direct, long-distance ET.[18] On the basis of the dependence of the long-distance ET rate on the nature and energy of the intervening porphyrin chromophore, they proposed that mixing of the π-orbitals of the porphyrin and chlorophyll leads to a state with charge transfer character which relaxes to the final IP state. They have further explored another set of triads where a keto functionality at the zinc pyropheophorbide is reduced to a secondary alcohol in order to lower its one-electron oxidation potential.[19] These models undergo a single step, long-distance, photoinduced ET within several picoseconds even at 77 K in 2-methyltetrahydrofuran.

Here we provide the synthesis and photophysical characterization of a new series of porphyrin–oxochlorin–pyromellitdimide (P–C–Im) triads **1**—**3** (Chart 1) in which the two macrocycles are held at a fixed distance (the center-to-center distance between P and C is ca. 12.8 Å) and orientation relative to each other with a 2,6-dimethoxy-1,4-phenylene bridge and the center-to-center distance between C and Im is fixed to be ca. 13 Å. Oxochlorin was originally prepared by Fisher almost 55 years ago[20] and has been increasingly employed in recent years in a variety of model studies including sulfite reductase siroheme and dissimilatory nitrite reductase heme d_1.[21—26] Here this macrocycle is employed because of its low one-electron reduction potential.[26] Pyromellitdimide electron acceptor is quite useful for analysis of ET kinetics and has a pertinent one-electron reduction potential for our purpose.[9] Of the triads studied here, photoexcitation of **2** in DMF results in formation of a long-lived charge separated state, $(ZnP)^+$–H_2C–$(Im)^-$, via the ET-relay depicted in Eq. 4 as a major route. Porphyrin–oxochlorin dyads **4**—**6**, and Im-linked and parent oxochlorins **7**—**10** were also prepared in order to understand the various events which follow from excitation of the triads. We have studied the excited-state dynamics of the triads in ben-

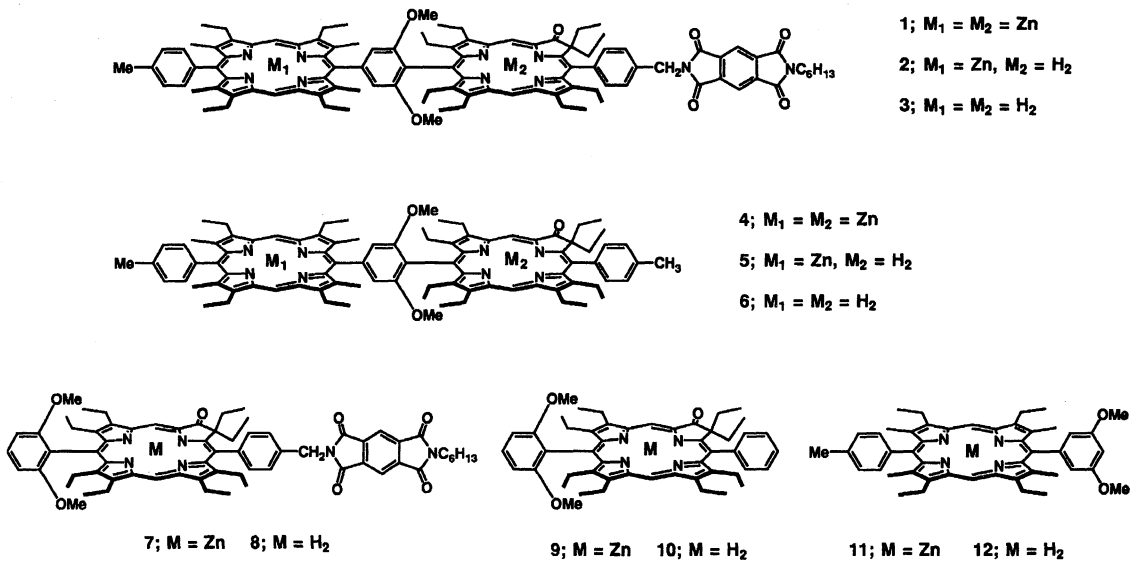

Chart 1. Structures of the models studied in this paper.

zene, THF, and DMF in order to investigate the solvent polarity effects. As discussed to some extent above and will be described in more detail later, the solvent polarity is an important parameter determining the excited-state dynamics of the models studied here.

Results and Discussion

Synthesis. Synthetic route to the triads **1**—**3** is outlined in Schemes 1 and 2. Pyromellitdimide-linked porphyrin **16** was prepared by cross condensation reaction of aldehydes **13** and **15** with tetraethyl-substituted dipyrrolylmethane **14** under our improved conditions.[27] The dimethoxy substituents at the *meso*-aryl ring in **16** were introduced in order to increase steric hindrance for OsO_4 oxidation at the near pyrrole rings, thereby effecting the oxidation regio-selectively at the opposite pyrrole rings. In fact, the oxidation of **16** followed by treatment with H_2S and acid-hydrolysis with trifluoroacetic acid gave pyromellitdimide oxochlorins **17** and **18**.[22] Oxidation products at the pyrrole ring near the dimethoxy-substituted aryl group were scarcely detected. The major oxidation product **17** was again condensed with p-tolualdehyde and dipyrrolylmethane **19** followed by zinc-insertion to give **1** in 20% yield. Demetalation with HCl gave **3** quantitatively, and treatment of **3** with an equimolar amount of $Zn(OAc)_2$ in a dichloromethane–methanol mixture at room temperature results in a selective metalation at the porphyrin to afford **2**. Pyromellitdimide-free reference molecules **4**—**6**, porphyrin-free molecules **7** and **8**, and parent oxochlorins **9** and **10** were prepared in essentially the same manner as for **1**—**3**. The ^1H NMR spectra of these models are nearly solvent independent, consistent with the expected constrained geometry of the two macrocycles.

Photophysics. The ground-state absorption spectra of **1**—**3** and **7**—**8** are almost solvent-independent and identical to the corresponding pyromellitdimide-free compounds **4**—**6** and **9**—**10**, respectively, indicating that attachment of the pyromellitdimide moiety to the macrocycles with a –phenyl–CH_2– spacer does not significantly perturb their electronic structure. The absorption spectra of **1**—**3** in THF are shown in Fig. 1. The ground-state absorption spectra in the Q-band region can be roughly described as a superposition of the respective spectra of the porphyrin (P) and oxochlorin (C) moieties, but those in the B-band region display broadening and red-shifting in **2** and **3** and a distinct splitting in **1**. The (0,0) Qy-band of C in **1**—**3** is observed at 635, 654, and 655 nm, respectively, and is 2—5 nm red-shifted from the respective bands in the reference molecules **9** (630 nm) and **10** (652 nm).[28] In the steady-state fluorescence spectra of **1**—**6**, only the emission bands from the oxochlorin moieties are commonly observed. The (0,0) emission band of ZnC in **1** is observed at 645 nm, being ca. 13 nm red-shifted from that (632 nm) in **9**, while the corresponding bands in **2**

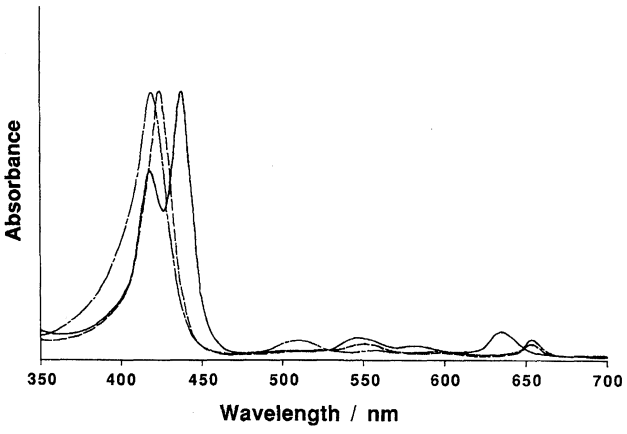

Fig. 1. Absorption spectra of **1** (—), **2** (– –), and **3** (–·–) in THF.

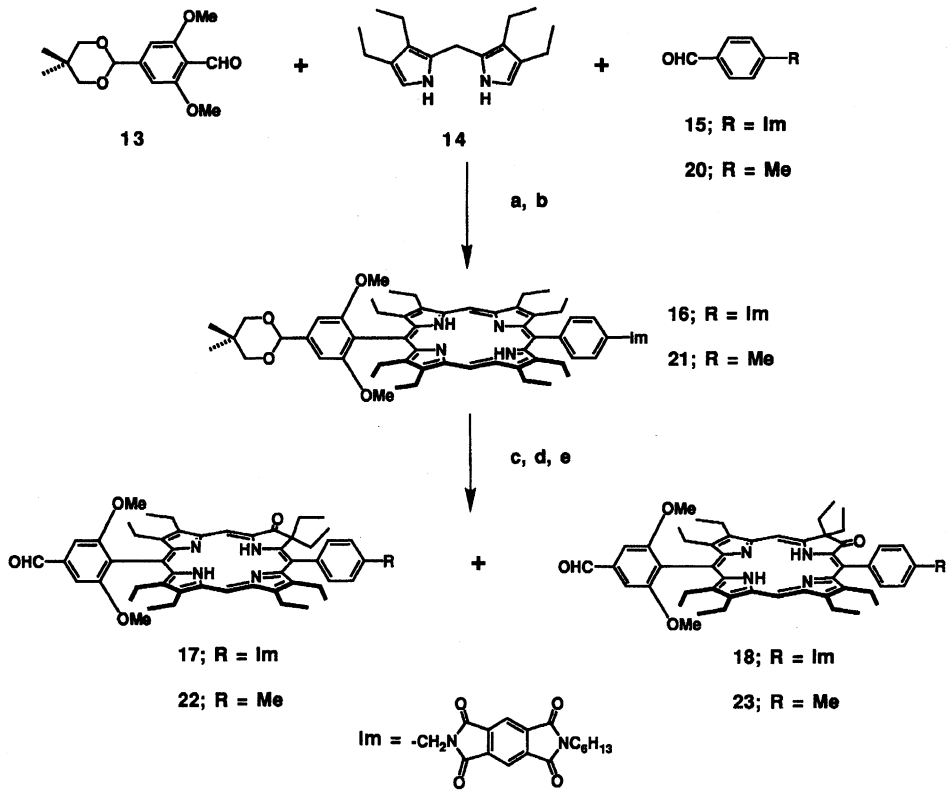

Scheme 1. Synthesis of oxochlorins **17**, **18**, **22**, and **23**. (a) CCl_3CO_2H, benzene–CH_3CN, room temperature 12 h. (b) *p*-chloranil, THF, room temperature, 6 h. (c) OsO_4, pyridine, ether–CH_2Cl_2, room temperature, dark, 3 d. (d) H_2S, CH_2Cl_2. (e) CF_3CO_2H, 10% H_2SO_4, refluxed, 10 h.

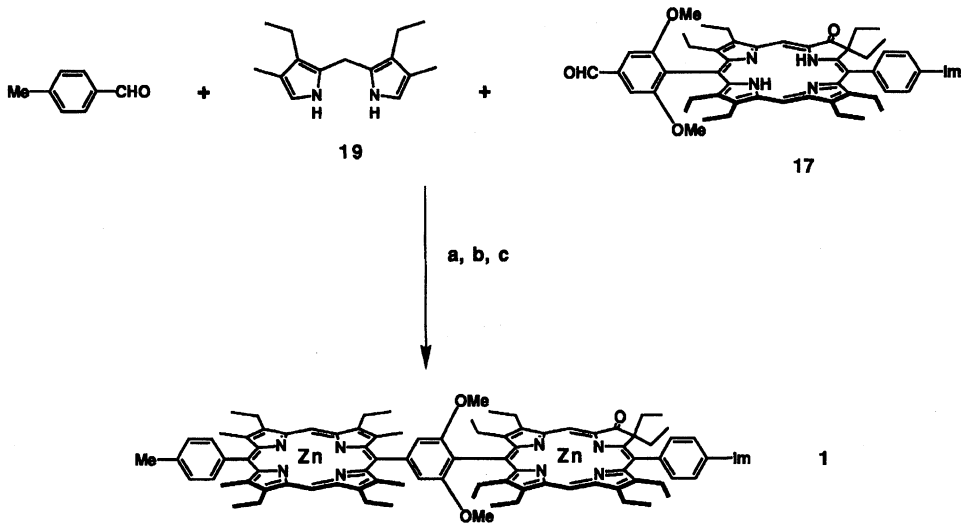

Scheme 2. Synthesis of triad **1**. (a) CCl_3CO_2H, CH_3CN, room temperature 6 h. (b) *p*-chloranil, THF, room temperature, 1 h. (c) $Zn(OAc)_2$, CH_2Cl_2–MeOH, reflux, 1 h.

and **3** are observed at 654 and 655 nm, respectively, and are red-shifted by merely 1-2 nm from that (653 nm) in **10**. Thus, we may conclude that there is substantial electronic coupling between the ZnP and ZnC moieties in **1** and **4** but that the π-electronic systems of the two macrocycles in **2**, **3**, **5**, and **6** are only weakly coupled in their S_1-states. Of these, the fluorescence spectra of **2** and **5** are solvent-polarity dependent. In Fig. 2, the fluorescence spectra of **2** and **5** in THF and DMF are shown along with the fluorescence spectrum of a 1:1 mixture of **10** and **11**. It is evident that the relative fluorescence yields from the $^1(H_2C)^*$ in **2** and **5** are decreased in DMF in comparison with those in THF or that of the mixture of **10** and **11**. These phenomena will be discussed in detail later.

Table 1 lists the energy levels of the locally excited

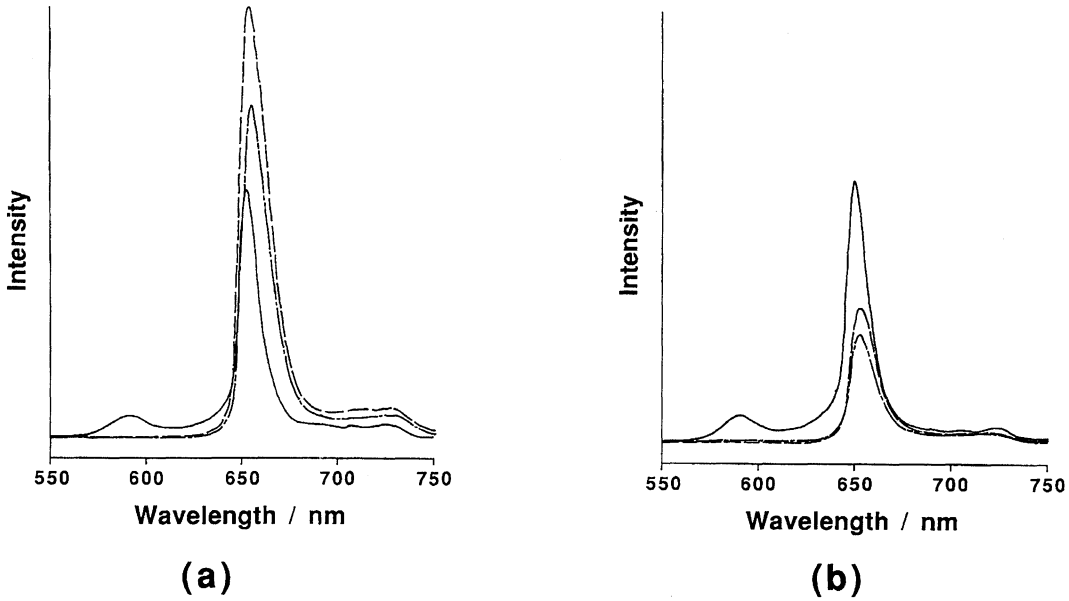

Fig. 2. Steady-state fluorescence spectra of **2** (-·-), **5** (---), and a 1:1 mixture of **10** and **11** (—). (a) In benzene and (b) in DMF. Absorbances at the excitation wavelength (420 nm) were adjusted to be 0.70.

Table 1. Estimated Energy Level (eV) for Low-Lying Locally Excited States and Charge Separated States

	Benzene	THF	DMF
$^1(H_2P)^*$	1.97	1.98	1.97
$^1(ZnP)^*$	2.13	2.13	2.16
$^1(H_2C)^*$	1.90	1.90	1.91
$^1(ZnC)^*$	1.96	1.97	1.96
$(H_2C)^+$–$(Im)^-$	2.52	1.88	1.68
$(ZnC)^+$–$(Im)^-$	2.25	1.61	1.41
$(H_2P)^+$–$(H_2C)^-$	2.42	2.10	1.97
$(ZnP)^+$–$(H_2C)^-$	2.31	1.88	1.76
$(ZnP)^+$–$(ZnC)^-$	2.54	2.11	1.99
$(H_2P)^+$–C–$(Im)^-$	2.52	1.88	1.64
$(ZnP)^+$–C–$(Im)^-$	2.49	1.70	1.43

The energies of the excited states are determined on the basis of the corresponding fluorescence and absorption (0,0) bands. The energies of the ion pair states in DMF were a simple sum of the electrochemical potential of the respective chromophore; the one-electron oxidation potentials of H_2P, ZnP, H_2C, and ZnC are 0.40, 0.19, 0.44, and 0.17 V, and the one-electron reduction potentials of H_2C, ZnC and Im are −1.57, −1.80, and −1.24 V vs. ferrocene/ferrocenium ion. The energies of the ion pair states in C_6H_6 and THF were estimated by: $E(\mathrm{IP})=E_{ox}-E_{red}+\Delta G_s$, $\Delta G_s=(e^2/2)(1/r_D+1/r_A)-(1/4\pi\varepsilon_0\varepsilon-1/4\pi\varepsilon_0\varepsilon_r)-e^2/4\pi\varepsilon_0\varepsilon R_{DA}$, where E_{ox} and E_{red} are oxidation and reduction potentials of donor and acceptor, respectively, measured in DMF, r_D and r_A are effective radii of donor cation and acceptor anion, ε_r and ε are dielectric constants of DMF and benzene or THF, respectively. The radii of $(P \text{ or } C)^+$, $(C)^-$, and $(Im)^-$, were taken to be 5, 5, and 3.5 Å, respectively, and the separation (R_{DA}) between charges to be. 12.8 Å for $(P)^+$–$(C)^-$, 13.0 Å for $(C)^+$–$(Im)^-$, and 24.4 Å for $(P)^+$–C–$(Im)^-$, respectively.

states of the chromophores within **1**—**12** along with several of their hypothetical IP states. The energies of the excited states are determined by averaging the energies of the corresponding (0,0) peaks in the fluorescence and absorption bands in each solvent. The energies of the IP states in DMF are estimated from a simple sum of the one-electron oxidation and reduction potentials of the donors and acceptors, while those in benzene and THF are estimated with corrected solvation energies calculated by the Born equation.[29] The calculated IP state energies in DMF may be reasonably good estimates of the true IP state energies, because the ions are strongly solvated and Coulombic interactions between ions are small. On the other hand, the estimates in less polar THF or benzene, especially in benzene, should be regarded as a rough estimate, since the estimation of the IP energy by the Born equation usually overestimates the correction term in low dipolar solvents as noted previously.[9]

Photoexcited-State Dynamics. In order to understand sometimes complicated photochemistry of the triads, it is appropriate to consider first some simpler compounds which constitute parts of the triads. We begin by discussing intramolecular photoinduced electron-transfer reactions in **7** and **8**.

Dyads 7 and 8. Fig. 3a shows the transient absorption spectra of **7** for excitation at 585 nm in benzene which reveal an efficient intramolecular CS producing an IP state $(ZnC)^+$–$(Im)^-$ and its CR to the ground state. Characteristic absorption at 718 nm due to $(Im)^-$ grows up with $\tau=180$ ps and decays with $\tau=2$ ns and time profile of the absorbance at 475 nm also contains 180-ps and 2-ns decaying components in addition to the constant one (Fig. 3b). These 180-ps and 2-ns components can be assigned to the decay of $^1(ZnC)^*$ and $(ZnC)^+$, respectively. Most of residual absorption around 470—480 nm at 5-ns delay time

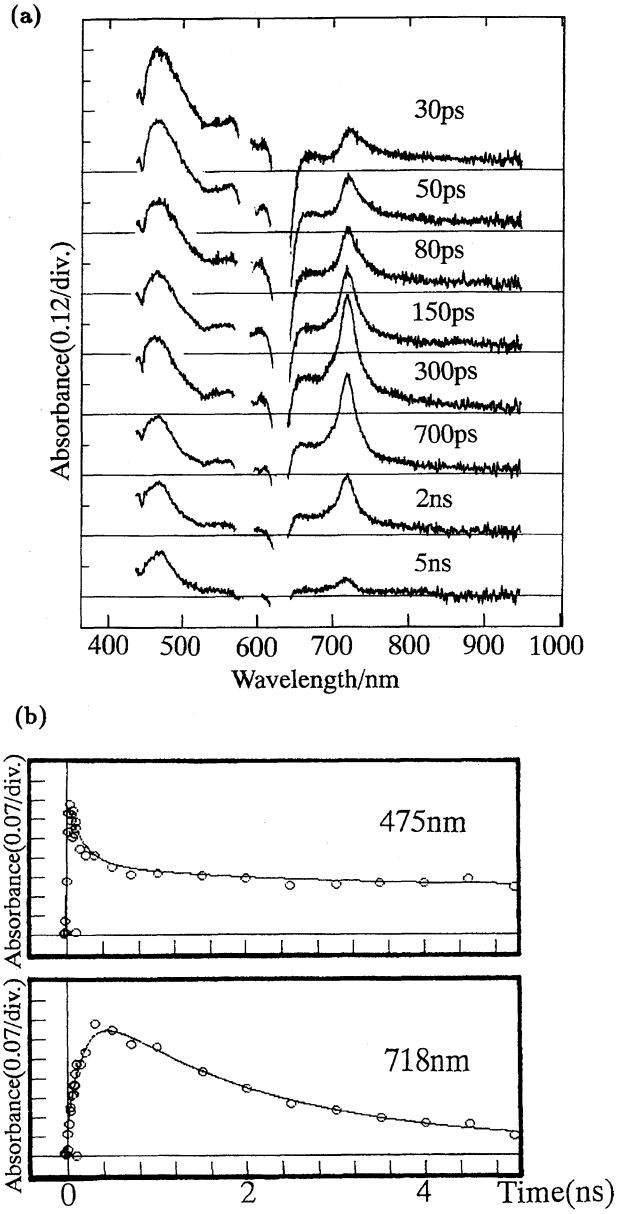

Fig. 3. (a) Time-resolved transient absorption spectra of **7** in benzene for excitation at 585 nm. (b) Time profiles in the transient absorption spectra of **7** in benzene at 475 (top) and 718 nm (bottom). The solid lines are the simulated curves by convolution of exciting pulse, transient absorption (see text), and probing pulse, assuming the lifetime of ^{1}(ZnC)*–Im (180 ps) and $(ZnC)^+$–$(Im)^-$ (2 ns).

that is responsible for the constant component in the time profile at 475 nm can be assigned to ^{3}(ZnC)* by comparing the relevant transient spectrum obtained for **9**. By simulating the observed kinetic traces at 475 and 718 nm, we have determined rates of both CS and CR in **7**; $k_{CS}=3.9\times10^9$ s^{-1} and $k_{CR}=5\times10^8$ s^{-1}.[9] In THF and DMF, similar but distinctly different transient absorption spectra (not shown) have been observed, which equally indicate the efficient CS leading to $(ZnC)^+$–$(Im)^-$ and the CR to the ground state in **7**. k_{CS} and k_{CR} values in THF and DMF determined in the same way are listed in Table 2. Fluorescence lifetimes of **7** and **9** were also used to calculate k_{CS} values (Table 2), which are in agreement with rates determined on the basis of the transient absorption data. It may be readily seen that k_{CS} is nearly solvent-polarity independent in contrast to CR which shows a large decrease in rate with decreasing solvent polarity. Similar solvent polarity effects on the CR of IP was first demonstrated with picosecond spectroscopy in the case of porphyrin–quinone systems (unlinked as well as linked by flexible chains)[30] that exhibit ultrafast CR decay in polar solvents. These results indicate the crucial importance of the multi-step ET strategies for attaining the long-lived IP state in the model systems involving porphyrin–quinone chromophores.[30] Similar solvent effects closely related to those in the present work were observed also in distance-fixed porphyrin–quinone[31] and porphyrin–pyromellitdimide dyads[9] and other distance-fixed dyads,[32] and can be qualitatively accounted for as follows. In these systems, the CS reaction is likely in the normal region, while the CR reaction in the IP state lies in the inverted region. With a decease of the solvent polarity, free energy gap for CS reaction decreases while the reorganization energy also decreases owing to diminished contribution from the solvent reorganization. Therefore, k_{CS} is not much affected by change in solvent polarity. However, in the CR reaction of the IP state, the free energy gap increases with a decrease of the solvent polarity, which results in a drastic decrease in k_{CR}.

On the other hand, the steady-state fluorescence from $^1(H_2C)^*$ in **8** is scarcely quenched in benzene and is only slightly quenched in THF and DMF by the attached Im. This has been also confirmed by measurement of fluorescence lifetimes (the fluorescence lifetimes of **8** and **10** are 6.2 and 6.2 ns in benzene, 4.7 and 6.3 ns in THF, and 5.3 and 6.5 ns in DMF, respectively). Given the observed reduction in the fluorescence lifetime of **8** in THF and DMF solely arising from CS between the $^1(H_2C)^*$ and Im, the k_{CS} values may be calculated to be 6.1×10^7 and 3.5×10^7 s^{-1} in THF and DMF, respectively. However, the transient absorption spectra taken for excitation of **8** in benzene, THF, and DMF are virtually the same as those for the Im-free reference **10**, featuring an instantaneous formation of $^1(H_2C)^*$–Im followed by the intersystem crossing to $^3(H_2C)^*$–Im with time constants which are nearly the same as observed in **10**. Accordingly, we may conclude that the CS between $^1(H_2C)^*$ and Im are inefficient even in polar DMF solution and does not lead to an accumulation of an IP state $(H_2C)^+$–$(Im)^-$ even if it actually occurs to some extent.

Dyads 4—6. The fact that the steady-state fluorescence spectra of **4**—**6** display only the emissions from the singlet excited state of the oxochlorin moiety, ^{1}(ZnC)* or $^1(H_2C)^*$ (in the case of **5**, see Fig. 2)

Table 2. Electron Transfer Rate Constants k_{CS} and k_{CR} in **7** and **8**[a)]

	7						**8**					
	k_{CS}[b)]	k_{CR}[b)]	k_{CS}[c)]	τ(ps)	τ_0(ps)	ϕ[d)]	k_{CS}[b)]	k_{CR}[b)]	k_{CS}[c)]	τ(ns)	τ_0(ns)	ϕ[e)]
Benzene	3.9×10^9	5×10^8	4.2×10^9	170	600	0.38	—	—	—	6.2	6.2	1.0
THF	3.9×10^9	2×10^{10}	6.9×10^9	120	460	0.19	$<10^8$	Nd[f)]	5.4×10^7	4.7	6.3	0.79
DMF	3.9×10^9	$>5\times10^{10}$	4.3×10^9	180	530	0.25	$<10^8$	Nd[f)]	2.7×10^7	5.3	6.5	0.81

a) Unimolecular rate, s^{-1}. b) Determined on the basis of the transient absorption spectra. c) Determined on the basis of the fluorescence lifetime, using the following equation; $k_{CS}=1/\tau-1/\tau_0$, where τ is the fluorescence lifetime of **7** or **8** and τ_0 is that of **9** or **10**. d) Relative fluorescence quantum yield to that of **9**. e) Relative fluorescence quantum yield to that of **10**. f) Not determined.

suggests the occurrence of efficient intramolecular singlet–singlet excitation energy transfer from the P to the C.[33)] Picosecond time resolved fluorescence measurements detect the short-lived fluorescence emission from the P. Measurements of fluorescence lifetime for these short-lived emissions were carried out by exciting at wavelength where absorption was due mainly to the P, at 575 nm for **4** and **5** and at 600 nm for **6**. The ^{1}(ZnP)* in **4** and **5** have a short lifetime of about 10 ps and the $^1(H_2P)^*$ in **6** has a lifetime of ca. 40—50 ps (Table 3). The reduction in the fluorescence lifetimes of the ^{1}(P)* can be ascribed solely to the occurrence of the intramolecular energy transfer to the C, since the fluorescence excitation spectra taken by monitoring fluorescence emission from the ^{1}(C)* are completely superimposable to the absorption spectra. On the basis of the fluorescence lifetimes thus measured, one can estimate rates of intramolecular excitation energy transfer (k_{EN}) by the following equation; $k_{EN}=1/\tau(P)-1/\tau_0(P)$, where τ(P) is the fluorescence lifetime of P in **4**—**6** and τ_0(P) is the fluorescence lifetime of **11** or **12**. Accordingly, values of ca. 1—1.5×10^{11} s^{-1} are estimated for k_{EN} in **4** and **5** and values of ca. 2—2.5×10^{10} s^{-1} are estimated for k_{EN} in **6**. Specific solvent dependence of k_{EN} has not been observed. Of the series **4**—**6**, the hybrid dimer **5** (ZnP–H_2C) is the only compound that shows solvent polarity dependent fluorescence quantum yields of the ^{1}(C)*. This is illustrated in Fig. 2. This comparison reveals that the fluorescence emission quantum yield from the $^1(H_2C)^*$ is enhanced in THF by the intramolecular EN from the ZnP to the H_2C, while it is significantly decreased in polar DMF solution. The fluorescence excitation spectrum of **5** in DMF monitored at the 655-nm region, where fluorescence is due entirely to the H_2C, reveals that the quantum yield of the EN from the ZnP to the H_2C is still very high. Thus, the reduction in the fluorescence quantum yield of the $^1(H_2C)^*$ must be associated with some additional, nonradiative decaying pathway. The reduction in fluorescence quantum yields of the $^1(H_2C)^*$ closely parallels the observed decrease in the fluorescence lifetime as the solvent polarity increases from benzene to DMF. Time-resolved fluorescence studies were again performed for **5** with excitation at 645 nm where absorption is due entirely to the H_2C. Fluorescence decay of **5** at 720 nm, where emission is due entirely to the $^1(H_2C)^*$, could not be satisfactorily reproduced by a single-exponential function, while a biexponential function gave a reasonably good agreement with $\tau_1=0.84$ ns (9%) and $\tau_2=5.34$ ns (91%) in benzene, $\tau_1=0.75$ ns (9%) and $\tau_2=5.28$ ns (91%) in THF, and $\tau_1=1.78$ ns (88%) and $\tau_2=5.04$ ns (12%) in DMF. The non single-exponential fluorescene-decay behavior of **5** remains to be explored but comparison of these emission data strongly indicates that the increase of the solvent polarity leads to an increase in rate of a new nonradiative channel for the $^1(H_2C)^*$ that competes with its radiative decay.

Table 3. Fluorescence Lifetime (ps) of the Porphyrin Moieties in **1**—**6**.

Model	**1**	**2**	**3**	**4**	**5**	**6**
Benzene	6	9	49	7	12	50
THF	10	6	53	12	8	39
DMF	10	8	51	11	11	39

Fluorescence lifetimes of **1**, **2**, **4**, and **5** were measured at 595 nm for excitation at 575 nm and those of **3** and **6** were measured at 620 nm for excitation at 600 nm.

Figures 4 and 5 show the transient absorption difference spectra of **5** at 100-ps and 6-ns delay time in benzene and DMF, respectively, obtained upon laser excitation at 645 nm. In the both solvents the Qy-band of H_2C at 655 nm bleaches immediately upon excitation. In benzene, absorbances at 450, 544, 574, and 620 nm and an induced emission at 728 nm in the spectrum at 100-ps delay time feature the $S_n\leftarrow S_1$ absorption of H_2C and spectral changes from 100-ps to 6-ns delay times are very small and are virtually the same as those taken for **10** (not shown). This indicates that ZnP–$^1(H_2C)^*$ decays via the same decaying channels available for **10** and that there is no evidence for formation of a $(ZnP)^+$–$(H_2C)^-$ ion-pair state. On the other hand, the spectral changes from 100-ps delay time to 6-ns delay time in DMF are large (Fig. 5). Particularly the absorbance at 450 nm where $^1(H_2C)^*$ have the maximum absorption coefficient decays faster with $\tau=2.3$ ns in **5**. These spectral changes, which are in line with the observed decreases in the fluorescence quantum yield and in the fluorescence lifetime of $^1(H_2C)^*$, seems to indicate an intramolecular CS giving $(ZnP)^+$–$(H_2C)^-$ in

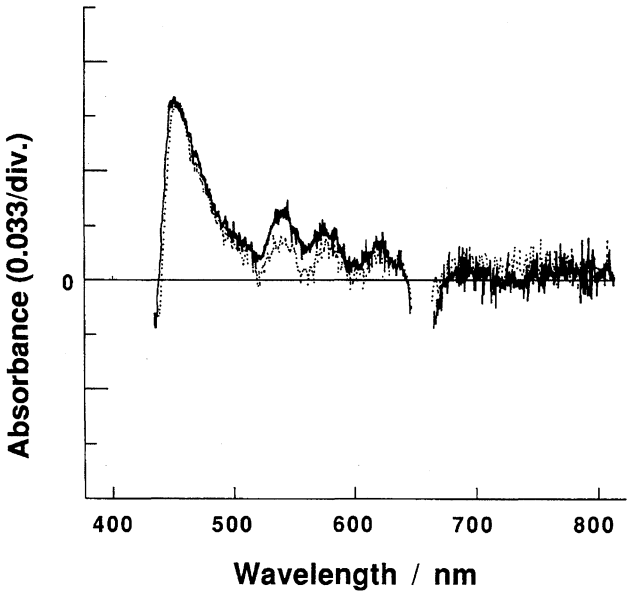

Fig. 4. Time-resolved transient absorption spectra of **5** in benzene for excitation at 645 nm, (—) at 100 ps and (····) at 6 ns delay times, respectively.

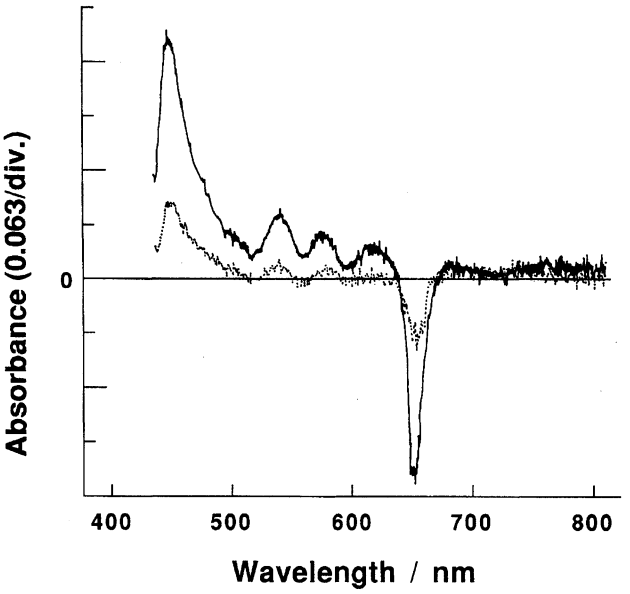

Fig. 5. Time-resolved transient absorption spectra of **5** in DMF for excitation at 645 nm, (—) at 100 ps and (····) at 6 ns delay times, respectively.

polar DMF solution, although it is indeed very difficult to assign these featureless spectra. Unfortunately, characteristic absorption around 670 nm due to $(ZnP)^+$ cannot be clearly detected owing to strong bleaching of the Qy-band of the $^1(H_2C)^*$. As discussed in the preceding section, CR reaction of IP state in the inverted region is usually very rapid in polar environment.[31,32,34,35] This may be the case for a $(ZnP)^+$–$(H_2C)^-$ IP state in DMF, thereby precluding its unambiguous detection. Assuming this CS to be the sole additional decaying pathway in the $^1(H_2C)^*$ in **5**, a rate ($k_{CS'}$) of CS from ZnP–$^1(H_2C)^*$ to $(ZnP)^+$–$(H_2C)^-$ can be estimated by the equation of $k_{CS'} = 1/\tau(H_2C) - 1/\tau_0(H_2C)$, where $\tau(H_2C)$ and $\tau_0(H_2C)$ are the lifetime of the $^1(H_2C)^*$ in **5** and **10**, respectively. Using the lifetimes of 2.3 and 6.5 ns for that of **5** and **10**, a $k_{CS'}$ value is calculated to be 2.9×10^8 s^{-1}.

Rate constant ($k_{CR'}$) of CR in the $(ZnP)^+$–$(H_2C)^-$ IP state can be estimated by referring to results of the energy gap ($-\Delta G_{CR}$) dependence of CR rate constants experimentally determined.[31,32] On the basis of the bell-shaped CR rate vs. $-\Delta G_{CR}$ relation for the loose geminate IP's in acetonitrile[34] which has static dielectric constant close to that of DMF and the E(IP) ($=-\Delta G_{CR}$)=1.76 eV in Table 1, the estimated $k_{CR'}$ value seems to be close to 10^{11} s^{-1}. However, due to the larger optical dielectric constants of DMF and probably weaker solvation of $(ZnP)^+$–$(H_2C)^-$ than that for the loose geminate IP's employed for obtaining the bell-shaped energy gap relation,[34] solvent reorganization energy λ_S associated with the CS from ZnP–$^1(H_2C)^*$ to $(ZnP)^+$–$(H_2C)^-$ in DMF should be considerably smaller than those for the geminate IP system. Weaker solvation of $(ZnP)^+$–$(H_2C)^-$ is reasonably expected by considering delocalized charge in radical ions over large, conjugated π-electronic systems vs. rather localized charges in radical ions in the loose geminate IP experiments. Owing to these effects on λ_S, the value of $k_{CR'}$ in $(ZnP)^+$–$(H_2C)^-$ may be smaller than that estimated above presumably by an order of magnitude (ca. 10^{10} s^{-1}) but still much larger than $k_{CS'}$.

Moreover, studies on the energy gap dependence of the CR for the distance-fixed porphyrin–quinone dyads suggested a minor role of solvent reorganization compared with the effect of high frequency quantum modes in the inverted region, where the CR rate vs. $-\Delta G_{CR}$ relation in THF was practically the same as that in benzene.[31] Given the same energy gap dependence of the CR rate in DMF solution, $k_{CR'}$ is estimated to be ca. 5×10^9 s^{-1} which is still an order of magnitude larger than $k_{CS'}$. If we consider the effect of λ_S to some extent in strongly polar solvent DMF, $k_{CR'}$ becomes much larger. In either case, direct observation of the IP state $(ZnP)^+$–$(H_2C)^-$ should be very difficult in DMF.

The excited-state dynamics of the $^1(C)^*$ in **4** and **6** are found to be almost solvent-polarity independent in benzene, THF, and DMF. The transient absorption spectra of **4** and **6** taken for selective excitation at C exciting at 645 nm are both very similar to those for **9** and **10**, respectively, and there is no evidence for CS within **4** and **6** in the three solvents examined.

Triads 1—3. As is the case with **4**—**6**, the steady-state fluorescence spectra display the emission only from $^1(C)^*$ (in the case of **2**, see Fig. 2), indicating again efficient singlet-singlet EN from $^1(P)^*$ to C in **1**—**3**. Photoexcited-state dynamics of P–$^1(C)^*$–Im thus formed are found to be dependent upon both the entities of P and C as well as the polarity of solvent. First,

the intramolecular electron-transfer reactions in **2** are described. The fluorescence emission from the $^1(H_2C)^*$ in **2** displays solvent-polarity dependent fluorescence quantum yield in a manner similar to that in **5** (Fig. 2), indicating the presence of additional nonradiative decaying pathway for the $^1(H_2C)^*$ in DMF. Figure 6 shows the transient absorption spectra of **2** in DMF for excitation at 645 nm. The characteristic absorptions as well as the induced emission due to $^1(H_2C)^*$ were observed immediately upon laser-pulse excitation. The absorbance at 460 nm decays with $\tau=1.8$ ns and the absorption at 716 nm characteristic of $(Im)^-$ rises with the same time constant of 1.8 ns. In the spectrum at 6-ns delay time, the long-lived absorption due to the $(Im)^-$ and bleachings at 560 and 595 nm due to $(ZnP)^+$ clearly indicate the formation of a stable, long-lived IP state $(ZnP)^+$–H_2C–$(Im)^-$. In Table 4, the decay time constants of $^1(H_2C)^*$ determined by the measurement

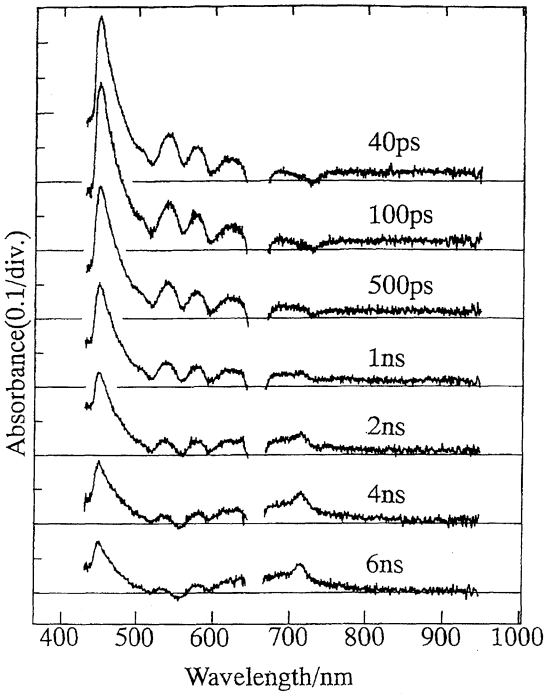

Fig. 6. Time-resolved transient absorption spectra of **2** in DMF for excitation at 645 nm.

Table 4. Decay Data of the Oxochlorin Moieties in DMF

Model	Fluorescence lifetime[a)]	$\tau(H_2P^*)$[b)]
10	6.46 (100)	>5
8	5.27 (100)	>5
5	1.78 (88.3), 5.04 (11.7)	2.3
2	1.46 (93), 4.08 (7)	1.8

a) Fluorescence lifetime measured at 700 nm for excitation at 645 nm (±5%). Numbers in parentheses are the relative amplitudes of pre-exponential factor. b) Decay time constants of the $^1(H_2C)^*$ determined by simulation of the observed time profile at 450 nm in the transient absorption spectrum for excitation at 645 nm, assuming a single exponential decay.

of the fluorescence lifetime or the transient absorption spectroscopy are summarized. The fluorescence decay curves of **8** and **10** can be fit with a single exponential function, while those of **2** and **5** are only satisfactorily deconvoluted with a double exponential function with a minor component of longer decaying time. Discrepancies between the data obtained by the two different measurements are relatively small and the decay time determined by transient absorption measurements for **2** and **5** agree reasonably well with those of the major components in the fluorescence lifetime measurements, respectively. Since the CS between the $^1(H_2C)^*$ and Im is much slower than the rise of the absorbance at 716 nm, it is concluded that $(ZnP)^+$–H_2C–$(Im)^-$ IP state is principally formed via a reaction scheme of ZnP–$^1(H_2C)^*$–Im→$(ZnP)^+$–$(H_2C)^-$–Im→$(ZnP)^+$–H_2C–$(Im)^-$. The other route by way of ZnP–$^1(H_2C)^*$–Im→ZnP–$(H_2C)^+$–$(Im)^-$→$(ZnP)^+$–H_2C–$(Im)^-$ might contribute for the formation of the final IP state but this contribution must be very minor. Inspection of Table 3 shows that the fluorescence lifetimes of the ZnP in **2** are all slightly shorter than those in **5**. Although this may suggest the occurrence of direct, long-distance ET from the $^1(ZnP)^*$ to the Im to some extent, corresponding rapid accumulation of $(ZnP)^+$–H_2C–$(Im)^-$ was not observed within such a short delay time in the transient absorption spectra for excitation at 532 nm. By using the respective difference absorption coefficients, ε(ZnP–$^1(H_2C)^*$–Im)$_{445}=17000$ (determined in this work) and $\varepsilon((ZnP)^+$–H_2C–$(Im)^-)_{715}=33000$,[12] we have estimated the quantum yield of 0.09 for the formation of $(ZnP)^+$–H_2C–$(Im)^-$ from ZnP–$^1(H_2C)^*$–Im. In this estimation the amount of ZnP–$^1(H_2C)^*$–Im formed by the incident light was determined by extrapolation of the absorbance at 445 nm to 0 delay time. Finally, the lifetime of the $(ZnP)^+$–H_2C–$(Im)^-$ IP state was determined to be 0.24 μs by the nano-to-microsecond transient absorption spectroscopy.

The estimated energy levels of the locally excited states and the hypothetical IP states in **2** are shown schematically in Scheme 3 along with conceivable reaction pathways. After efficient singlet-singlet EN (path 3), intramolecular CS occurs from ZnP–$^1(H_2C)^*$–Im to give an initial IP state $(ZnP)^+$–$(H_2C)^-$–Im (path 4) and following CSH reaction results in the formation of a final IP state $(ZnP)^+$–H_2C–$(Im)^-$ (path 7), in competition with the CR to the ground state (path 6). Following the same method as for **5**, k_4 (tentatively designated as $k_{CS'}$ in the case of **5**) is calculated to be 3.7×10^8 s^{-1}, being roughly the same value as found in **5**. The final IP state is fairly long-lived with a lifetime of 0.24 μs and undergoes a slow CR to the ground state (path 10) once formed. The final IP state $(ZnP)^+$–H_2C–$(Im)^-$ might be provided by other ET-relay (steps 5 and 8) as a minor route, provided that hole transfer reaction (step 8) could compete with CR to the ground state (step 9). Assuming the reaction scheme in Scheme 3,

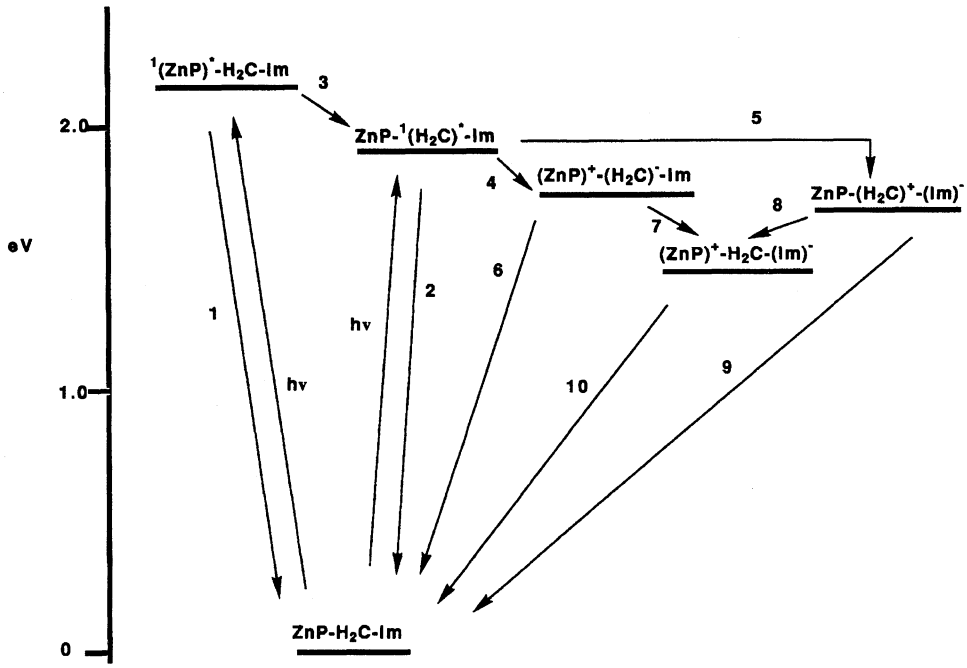

Scheme 3. Reaction scheme and energy diagram for **2** in DMF.

the quantum yield for formation of $(ZnP)^+$–$(H_2C)^-$–Im from ZnP–$^1(H_2C)^*$–Im is $k_4/(k_2+k_4+k_5)$, and therefore is calculated to be 0.67, using $k_2=1.5\times10^8$ s^{-1}, $k_4=3.7\times10^8$ s^{-1}, and $k_5=2.7\times10^7$ s^{-1}. Similarly, the quantum yield for formation of ZnP–$(H_2C)^+$–$(Im)^-$ from ZnP–$^1(H_2C)^*$–Im is calculated to be 0.05.

It should be noted here that the decay time of (ZnP)–$^1(H_2C)^*$–Im and the rise time of the final IP state $(ZnP)^+$–H_2C–$(Im)^-$ determined by the time-resolved absorption spectral measurements were practically the same (1.8 ns). Although the rate constant of the CSH reaction, k_7, is not clear, the value of k_6 seems to be much larger (ca. 10^{10} s^{-1}) than the decay rate constant (5.5×10^8 s^{-1}) of $^1(H_2C)^*$, considering the rough estimation of k_6 given in the previous section. Therefore, the rise time of the final IP state is practically determined by the decay time of ZnP–$^1(H_2C)^*$–Im state. By assuming this k_6 value and using the quantum yields of the final IP state (0.09), k_7 is estimated to be ca. 10^9 s^{-1}. Although the contribution of the ZnP–$(H_2C)^+$–$(Im)^-$ state to the final IP state formation seems negligibly small, a rough estimate of the CR rate constant of this intermediate IP state (k_9) can be made by the procedure similar to the case of k_6, which gives k_9 ca. 10^{10}—10^{11} s^{-1}.

The sequential ET-relay (steps 4 and 7) observed for **2** in DMF partly duplicates the primary ET events in the RC in the sense that the initial CS takes place between tetrapyrrole pigments and then the electron shifts to the acceptor. To our knowledge, this is the first example in which such an ET-relay has been clearly demonstrated to proceed in a single molecule. However, the quantum yield leading to $(ZnP)^+$–H_2C–$(Im)^-$ is rather low. As described above, the polarity of solvents is an important parameter in determining the course and efficiency of ET-relay in these triads. Inspection of Table 1 reveals that in DMF the energy level of $(ZnP)^+$–$(H_2C)^-$–Im IP state is slightly higher than that of ZnP–$(H_2C)^+$–$(Im)^-$. The energy gaps for charge separations leading to these states from the ZnP–$^1(H_2C)^*$–Im state are 0.15 eV for the former IP and 0.23 eV for the latter, respectively. Probably these charge separations are lying in the normal region regarding the energy gap dependence of the reaction. Nevertheless the ZnP–$^1(H_2C)^*$–(Im) state preferentially undergoes a CS to the former IP state with a rate which is more than ten times larger than that to the latter. Perhaps this is due to the much larger reorganization energy associated with CS to the ZnP–$(H_2C)^+$–$(Im)^-$ IP state. It seems reasonable to expect that there is enhanced electron density at the oxygen atom in the anion radical of pyromellitdimide, which must be strongly solvated by polar solvents. In contrast, macrocyclic radical ion species such as $(ZnP)^+$, $(H_2C)^-$, and $(H_2C)^+$ are π-radical ion in nature and should have delocalized electron density over their macrocycles. Therefore, with the increase of solvent polarity, the increase in reorganization energy associated with step 4 can be smaller in comparison with that associated with step 5. A similar discussion is given also in the rough estimation of k_6 value. This may give rise to preferential CS of step 4 over step 5. It is also quite general that polar environment enhances rates of energy-wasteful steps 6 and 9. Although correct estimations of k_6 and k_9 are difficult, probably they are quite large in DMF as discussed above, thereby decreasing the total quantum yield for the formation of $(ZnP)^+$–H_2C–$(Im)^-$. This defect could be overcome by designing molecules with increased thermodynamic

driving force for step 4 so that it is possible even in nonpolar solvents.

Figure 7 shows the transient absorption spectra of **1** in THF for excitation at 645 nm. It is obvious that CS between the ^{1}(ZnC)* and Im provides an IP state ZnP–(ZnC)$^+$–(Im)$^-$ which decays to the ground state relatively rapidly within 500 ps. Deconvolution of the kinetic traces at 476 and 715 nm reveals that both CS and CR occur with rates which are nearly the same as those in **7** and there is no spectroscopic indication for a hole transfer leading to formation of (ZnP)$^+$–ZnC–(Im)$^-$. Essentially the same photoexcited-state dynamics were observed in benzene and DMF. These results may be ascribed to insufficient energy gaps for the hole transfer (Table 1). Excited-state dynamics of **3** were also found nearly solvent-polarity independent and are quite similar with those of **6** and **10**, except that the decay of ^{1}(H$_2$C)* in **3** is somewhat accelerated in THF and DMF. No indication has been obtained for formation of long-lived IP state.

Concluding Remarks

The results presented above show that a stepwise, sequential ET-relay leading to long-lived IP state is actually taking place in **2** dissolved in DMF. A kinetic investigation of these triads indicate that structural or environmental changes which affect some rate constants invariably affect others. Thus, rational molecular design of photosynthetic models needs a very detailed knowledge of effects upon a given structural or environmental perturbation. In particular, rather polar environment is necessary for the desired ET-relay but this requirement is accompanied by enhanced rates of the energy wasteful CR processes, decreasing the total quantum yield of the final, long-lived IP state. On the basis of these results as well as the earlier ones, we are approaching mimicry of ultrafast and highly efficient formation of long-lived IP states by way of a sequential ET-relay mimicking the primary ET reactions in the RC in a single molecule. Further works directed toward achieving these goals are currently underway in our laboratories and will be reported elsewhere.

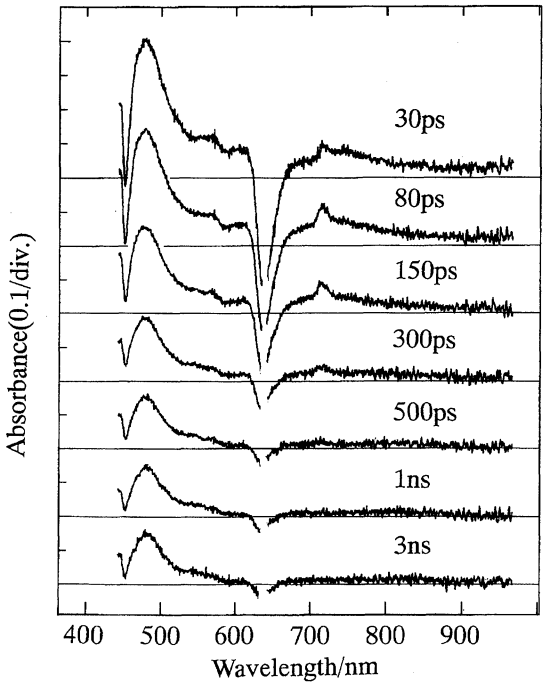

Fig. 7. Time-resolved transient absorption spectra of **1** in THF for excitation at 585 nm.

Experimental

Unless otherwise stated, all commercially available regents and solvents were used without further purification. Acetonitrile and dichloromethane were refluxed over and distilled from P_2O_5. Pyridine was distilled and stored over KOH. Preparative separations were performed usually by flash column chromatography on silica gel (Merck, Kieselgel 60H, Art. 7736).

^{1}H NMR spectra were recorded on a JEOL α-500 spectrometer (operating as 500 MHz) and chemical shifts were represented as δ-values relative to the internal standard TMS. UV-visible spectra were recorded on a Shimadzu UV-3000 spectrometer and steady-state fluorescence spectra were taken on an RF-502A spectrofluorimeter. Mass spectra were recorded on a JEOL HX-110 mass spectrometer. For porphyrin and oxochlorin compounds, the positive FAB (fast atom bombardment) ionization method was used, accelerating voltage 10 kV, Xe atom as the primary ion source. The FAB matrix was 3-nitrobenzyl alcohol. IR spectra (KBr method) were taken on a Horiba FT-3000 spectrometer.

Fluorescence lifetimes were measured on 10^{-7} M air-saturated solutions (1 M=1 mol dm^{-3}) with a picosecond time-correlated single-photon counting system.[36] Picosecond transient absorption spectra were measured by means of a microcomputer-controlled double-beam picosecond spectrometer with a repetitive mode-locked Nd^{3+}: YAG laser 24-ps pulse duration[37] or with a picosecond dye laser 8-ps pulse duration pumped by the second harmonic of a repetitive mode-locked Nd^{3+}: YAG laser.[38] The second harmonic of the Nd^{3+}: YAG laser pulse or the 620 nm output of the dye laser was used for excitation. A Q-switched Nd^{3+}: YAG laser (Quantel YG580) with the second harmonic output (532 nm, 15 ns pulse duration) of 40 mJ was used for measurements of nanosecond transient absorption spectra.[39]

Synthesis of 16. The di-(2-pyrrolyl)methane **14**[40] (2.47 g, 9.57 mmol), the aldehyde **13** (2.01 g, 7.17 mmol) and the pyromellitdimide-linked aldehyde **15**[41] (1.0 g, 2.39 mmol) were dissolved in a mixture of dry benzene (100 ml) and acetonitrile (100 ml). Trichloroacetic acid (500 mg, 3.06 mmol) was added to this solution, and the resulting solution was stirred for 12 h at room temperature under an Ar atmosphere in the dark. A solution of *p*-chloranil (3.53 g, 14.3 mmol) in THF (100 ml) was added and the resulting solution was stirred for an additional 6 h. After evaporation of the solvent, the residue was dissolved in CH_2Cl_2 (400 ml), and the resulting solution was successively treated with 3 M (1 M=1 mol dm^{-3}) HCl (400 ml) and saturated aqueous Na_2CO_3 solution (400 ml), and then dried over anhydrous Na_2SO_4. After metalation with $Zn(OAc)_2$, the porphyrin products were separated by flash column chromatography

on silica gel (MeOH-free CH_2Cl_2 eluent). Second porphyrin fraction was collected, treated with 3 M HCl, and washed with aqueous Na_2CO_3. After evaporation of the solvent, recrystallization from CH_2Cl_2/MeOH gave **16** as violet crystals (430 mg, 0.37 mmol) in 15% yield based on the amount of **15** used.

16. Mp >300 °C. ^{1}H NMR ($CDCl_3$) $\delta=-1.98$ (broad, 2H, NH), 0.90 (t, 3H, Hexyl-Me), 0.94 (s, 3H, Me), 1.10 (t, 6H, $J=7.6$ Hz, Et), 1.19 (t, 6H, $J=7.4$ Hz, Et), 1.34 (m, 6H, Hexyl-CH_2), 1.47 (s, 3H, Me), 1.72 (m, 2H, Hexyl-CH_2), 1.82 (t, 6H, $J=8.2$ Hz, Et), 1.86 (t, 6H, $J=8.2$ Hz, Et), 2.73 (q, 4H, $J=7.6$ Hz, Et), 3.03 (q, 4H, $J=7.4$ Hz, Et), 3.56 (s, 6H, OMe), 3.76 (t, 2H, Hexyl-CH_2), 3.85 (d, 2H, $J=11.0$ Hz, CH_2), 3.98 (d, 2H, $J=11.0$ Hz, CH_2), 3.98 (q, 8H, $J=8.2$ Hz, Et), 5.23 (s, 2H, Benzyl-CH_2), 5.73 (s, 1H, CH), 7.11 (s, 2H, Ar-H), 7.67 (d, 2H, $J=7.7$ Hz, Ar-H), 8.17 (d, 2H, $J=7.7$ Hz, Ar-H), 8.34 (s, 2H, Im-Ar-H), 10.16 (s, 2H, *meso*-H). HRMS(FAB): Found: m/z 1173.639. Calcd for $C_{73}H_{85}O_8N_6$: M^++H, 1173.643.

Porphyrin **21** was prepared from **13**, **14**, and **20** in 25% yield in the same manner as described for **16**.

21. Mp 297—299 °C. ^{1}H NMR ($CDCl_3$) $\delta=-1.91$ (broad, 2H, NH), 0.94 (s, 3H, Me), 1.18 (t, 6H, $J=7.5$ Hz, Et), 1.19 (t, 6H, $J=7.6$ Hz, Et), 1.47 (s, 3H, Me), 1.85 (t, 12H, $J=7.1$ Hz, Et), 2.72 (s, 3H, Tolyl-Me), 2.82 (q, 4H, $J=7.5$ Hz, Et), 3.04 (q, 4H, $J=7.6$ Hz, Et), 3.56 (s, 6H, OMe), 3.85 (d, 2H, $J=10.7$ Hz, CH_2), 3.99 (d, 2H, $J=10.7$ Hz, CH_2), 4.00 (q, 8H, $J=7.1$ Hz, Et), 5.73 (s, 1H, CH), 7.11 (s, 2H, Ar-H), 7.46 (d, 2H, $J=7.7$ Hz, Ar-H), 8.06 (d, 2H, $J=7.7$ Hz, Ar-H), 10.17 (s, 2H, *meso*-H). HRMS(FAB): Found: m/z 875.551. Calcd for $C_{57}H_{71}O_4N_4$: M^++H, 875.548.

Synthesis of Oxochlorin Monomers. Typically, the synthesis of **17** and **18**, which was carried out by a modification of the Chang's method,[22] was described. Dry pyridine (0.11 ml) was added to a dry ether (2.0 ml) solution of OsO_4 (110 mg, 0.435 mmol). The resultant yellow solution of OsO_4–pyridine complex was added to a solution of the porphyrin **16** (170 mg, 0.15 mmol) in dry CH_2Cl_2 (20 ml). The mixture was stirred for 3 d at room temperature under a dr Ar atmosphere in the dark. H_2S gas was passed through the mixture for 1 h so as to induce the precipitation of osmium sulfide. The resultant precipitate was filtered off. CF_3CO_2H (10 ml) and 10% H_2SO_4 (10 ml) were added to the filtrate. The resulting solution was refluxed for 10 h, and the reaction mixture was poured into water. The organic layer was separated, successively washed with water and aqueous Na_2CO_3, and dried over anhydrous Na_2SO_4. After evaporation of the solvent, the oxochlorin isomers were separated by silica gel flash column chromatography (benzene/Et_2O (98/2) eluent). Each isomer was precipitated from CH_2Cl_2/hexane, giving **17** (40 mg, 36.25 μmol, 26% yield) and **18** (10 mg, 9.06 μmol, 6% yield), respectively.

17. Mp 198—200 °C. ^{1}H NMR ($CDCl_3$) $\delta=-1.75$ (s, 1H, NH, the other NH was not detected), 0.24 (t, 6H, $J=7.3$ Hz, rearranged-Et), 0.90 (t, 3H, Hexyl-Me), 1.09 (t, 3H, $J=7.6$ Hz, Et), 1.11 (t, 3H, $J=7.1$ Hz, Et), 1.13 (t, 3H, $J=7.6$ Hz, Et), 1.34 (m, 6H, Hexyl-CH_2), 1.73 (m, 2H, Hexyl-CH_2), 1.77 (t, 3H, $J=7.5$ Hz, Et), 1.80 (t, 3H, $J=7.8$ Hz, Et), 1.84 (t, 3H, $J=7.5$ Hz, Et), 2.14 (m, 4H, $J=7.3$ Hz, rearranged-Et), 2.57 (q, 2H, $J=7.6$ Hz, Et), 2.82 (q, 2H, $J=7.6$ Hz, Et), 2.99 (q, 2H, $J=7.1$ Hz, Et), 3.64 (s, 6H, OMe), 3.78 (t, 2H, Hexyl-CH_2), 3.84 (q, 2H, $J=7.5$ Hz, Et), 3.96 (q, 2H, $J=7.8$ Hz, Et), 3.98 (q, 2H, $J=7.5$ Hz, Et), 5.23 (s, 2H, Benzyl-CH_2), 7.48 (s, 2H, Ar-H), 7.68 (d, 2H, $J=7.9$ Hz, Ar-H), 8.00 (d, 2H, $J=7.9$ Hz, Ar-H), 8.42 (s, 2H, Im–Ar-H), 9.95 (s, 1H, *meso*-H), 10.00 (s, 1H, *meso*-H), 10.30 (s, 1H, CHO). HRMS (FAB): Found: m/z 1103.570. Calcd for $C_{68}H_{75}O_8N_6$: M^++H, 1103.565. IR (KBr) ν_{max} 1720 cm^{-1} (CO, CHO, imide CO).

18. Mp 194—197 °C. ^{1}H NMR ($CDCl_3$) $\delta=-1.79$ (s, 1H, NH), −0.95 (broad, 1H, NH), 0.29 (t, 6H, $J=7.2$ Hz, rearranged-Et), 0.90 (t, 3H, Hexyl-Me), 1.08 (t, 3H, $J=7.7$ Hz, Et), 1.09 (t, 3H, $J=7.7$ Hz, Et), 1.14 (t, 3H, $J=7.7$ Hz, Et), 1.34 (m, 6H, Hexyl-CH_2), 1.74 (m, 2H, Hexyl-CH_2), 1.74 (t, 6H, $J=7.6$ Hz, Et), 1.78 (t, 3H, $J=7.6$ Hz, Et), 2.57 (m, 4H, $J=7.2$ Hz, rearranged-Et), 2.75 (q, 2H, $J=7.7$ Hz, Et), 2.78 (q, 2H, $J=7.7$ Hz, Et), 2.98 (q, 2H, $J=7.7$ Hz, Et), 3.66 (s, 6H, OMe), 3.78 (t, 2H, Hexyl-CH_2), 3.85 (q, 2H, $J=7.6$ Hz, Et), 3.88 (q, 2H, $J=7.6$ Hz, Et), 3.95 (q, 2H, $J=7.6$ Hz, Et), 5.22 (s, 2H, Benzyl-CH_2), 7.48 (s, 2H, Ar-H), 7.73 (d, 2H, $J=8.0$ Hz, Ar-H), 7.84 (d, 2H, $J=8.0$ Hz, Ar-H), 8.39 (s, 2H, Im–Ar-H), 9.06 (s, 1H, *meso*-H), 10.02 (s, 1H, *meso*-H), 10.30 (s, 1H, CHO). HRMS (FAB): Found: m/z 1103.554. Calcd for $C_{68}H_{75}O_8N_6$: M^++H, 1103.565. IR (KBr) ν_{max} 1718 cm^{-1} (CO, CHO, imide CO).

The oxochlorins **22** and **23** were prepared by the OsO_4 oxidation of **21** in 13 and 8% yields, respectively, in the same manner as described for **17** and **18**.

22. Mp >300 °C. ^{1}H NMR ($CDCl_3$) $\delta=-1.74$ (s, 1H, NH), −0.86 (broad, 1H, NH), 0.25 (t, 6H, $J=7.5$ Hz, rearranged-Et), 1.10 (t, 3H, $J=7.4$ Hz, Et), 1.14 (t, 3H, $J=7.6$ Hz, Et), 1.20 (t, 3H, $J=7.7$ Hz, Et), 1.77 (t, 3H, $J=7.6$ Hz, Et), 1.80 (t, 3H, $J=7.3$ Hz, Et), 1.85 (t, 3H, $J=7.6$ Hz, Et), 2.19 (m, 4H, $J=7.5$ Hz, rearranged-Et), 2.68 (s, 3H, Tolyl-Me), 2.71 (q, 2H, $J=7.7$ Hz, Et), 2.83 (q, 2H, $J=7.5$ Hz, Et), 2.99 (q, 2H, $J=7.6$ Hz, Et), 3.64 (s, 6H, OMe), 3.84 (q, 2H, $J=7.6$ Hz, Et), 3.99 (q, 2H, $J=7.3$ Hz, Et), 4.00 (q, 2H, $J=7.6$ Hz, Et), 7.45 (d, 2H, $J=7.9$ Hz, Ar-H), 7.49 (s, 2H, Ar-H), 7.89 (d, 2H, $J=7.9$ Hz, Ar-H), 9.96 (s, 1H, *meso*-H), 10.01 (s, 1H, *meso*-H), 10.31 (s, 1H, CHO). HRMS (FAB): Found: m/z 805.473. Calcd for $C_{52}H_{61}O_4N_4$: M^++H, 805.469. IR (KBr) ν_{max} 1707 cm^{-1} (CO, CHO).

23. Mp 201—203 °C. ^{1}H NMR ($CDCl_3$) $\delta=-1.77$ (s, 1H, NH), −0.95 (broad, 1H, NH), 0.30 (t, 6H, $J=7.2$ Hz, rearranged-Et), 1.09 (t, 3H, $J=7.6$ Hz, Et), 1.14 (t, 3H, $J=7.6$ Hz, Et), 1.21 (t, 3H, $J=7.4$ Hz, Et), 1.75 (t, 3H, $J=7.6$ Hz, Et), 1.76 (t, 3H, $J=7.4$ Hz, Et), 1.82 (t, 3H, $J=7.6$ Hz, Et), 2.58 (m, 4H, $J=7.2$ Hz, rearranged-Et), 2.67 (s, 3H, Tolyl-Me), 2.79 (q, 2H, $J=7.6$ Hz, Et), 2.91 (q, 2H, $J=7.4$ Hz, Et), 2.98 (q, 2H, $J=7.6$ Hz, Et), 3.66 (s, 6H, OMe), 3.81 (q, 2H, $J=7.6$ Hz, Et), 3.89 (q, 2H, $J=7.4$ Hz, Et), 3.99 (q, 2H, $J=7.6$ Hz, Et), 7.48 (s, 2H, Ar-H), 7.49 (d, 2H, $J=7.7$ Hz, Ar-H), 7.75 (d, 2H, $J=7.7$ Hz, Ar-H), 9.07 (s, 1H, *meso*-H), 10.04 (s, 1H, *meso*-H), 10.30 (s, 1H, CHO). HRMS (FAB): Found: m/z 805.459. Calcd for $C_{52}H_{61}O_4N_4$: M^++H, 805.469. IR (KBr) ν_{max} 1709 cm^{-1} (CO, CHO).

The oxochlorins **7** and **9** were prepared from appropriate porphyrin precursors essentially the same manner in ca. 50% yield and the free base oxochlorins **8** and **10** were prepared by usual acidic demetalation of **7** and **9** in quantitative yields, respectively.

7. Mp >300 °C. ^{1}H NMR ($CDCl_3$) δ=0.24 (t, 6H, J=7.2 Hz, rearranged-Et), 0.90 (t, 3H, Hexyl-Me), 1.01 (t, 3H, J=7.4 Hz, Et), 1.07 (t, 3H, J=7.6 Hz, Et), 1.09 (t, 3H, J=7.3 Hz, Et), 1.35 (m, 6H, Hexyl-CH_2), 1.71 (m, 2H, Hexyl-CH_2), 1.71 (t, 6H, J=7.6 Hz, Et), 1.75 (t, 3H, J=7.6 Hz, Et), 2.10 (m, 4H, J=7.2 Hz, rearranged-Et), 2.31 (q, 2H, J=7.4 Hz, Et), 2.80 (q, 2H, J=7.6 Hz, Et), 2.84 (q, 2H, J=7.3 Hz, Et), 3.55 (s, 6H, OMe), 3.78 (t, 2H, Hexyl-CH_2), 3.79 (m, 6H, Et), 5.20 (s, 2H, Benzyl-CH_2), 6.94 (d, 2H, J=8.4 Hz, Ar-H), 7.62 (d, 2H, J=7.9 Hz, Ar-H), 7.74 (t, 1H, J=8.4 Hz, Ar-H), 7.96 (d, 2H, J=7.9 Hz, Ar-H), 8.41 (s, 2H, Im–Ar-H), 9.96 (s, 1H, *meso*-H), 9.75 (s, 1H, *meso*-H). HRMS (FAB): Found: m/z 1136.477. Calcd for $C_{67}H_{72}O_7N_6Zn$: M^+, 1136.475. IR (KBr) ν_{max} 1714 cm^{-1} (CO, imide CO).

8. Mp 198—199 °C. ^{1}H NMR ($CDCl_3$) δ=−1.71 (s, 1H, NH, the other NH was not detected), 0.23 (t, 6H, J=7.3 Hz, rearranged-Et), 0.90 (t, 3H, Hexyl-Me), 1.10 (t, 3H, J=7.5 Hz, Et), 1.12 (t, 3H, J=7.3 Hz, Et), 1.15 (t, 3H, J=7.4 Hz, Et), 1.35 (m, 6H, Hexyl-CH_2), 1.73 (m, 2H, Hexyl-CH_2), 1.76 (t, 3H, J=7.6 Hz, Et), 1.79 (t, 3H, J=7.8 Hz, Et), 1.82 (t, 3H, J=7.8 Hz, Et), 2.13 (m, 4H, J=7.3 Hz, rearranged-Et), 2.57 (q, 2H, J=7.5 Hz, Et), 2.86 (q, 2H, J=7.3 Hz, Et), 3.02 (q, 2H, J=7.4 Hz, Et), 3.54 (s, 6H, OMe), 3.78 (t, 2H, Hexyl-CH_2), 3.83 (q, 2H, J=7.6 Hz, Et), 3.96 (q, 2H, J=7.8 Hz, Et), 3.97 (q, 2H, J=7.8 Hz, Et), 5.23 (s, 2H, Benzyl-CH_2), 6.94 (d, 2H, J=8.5 Hz, Ar-H), 7.67 (d, 2H, J=7.9 Hz, Ar-H), 7.75 (t, 1H, J=8.5 Hz, Ar-H), 8.00 (d, 2H, J=7.9 Hz, Ar-H), 8.42 (s, 2H, Im–Ar-H), 9.93 (s, 1H, *meso*-H), 9.98 (s, 1H, *meso*-H). HRMS (FAB): Found: m/z 1075.558. Calcd for $C_{67}H_{75}O_7N_6$: M^++H, 1075.570. IR (KBr) ν_{max} 1720 cm^{-1} (CO, imide CO).

9. Mp 192—194 °C. ^{1}H NMR ($CDCl_3$) δ=0.27 (t, 6H, J=7.3 Hz, rearranged-Et), 1.08 (t, 3H, J=7.7 Hz, Et), 1.09 (t, 3H, J=7.5 Hz, Et), 1.11 (t, 3H, J=7.5 Hz, Et), 1.73 (t, 6H, J=7.6 Hz, Et), 1.79 (t, 3H, J=7.5 Hz, Et), 2.15 (m, 4H, J=7.3 Hz, rearranged-Et), 2.41 (q, 2H, J=7.7 Hz, Et), 2.81 (q, 2H, J=7.5 Hz, Et), 2.85 (q, 2H, J=7.5 Hz, Et), 3.56 (s, 6H, OMe), 3.82 (q, 2H, J=7.6 Hz, Et), 3.83 (q, 4H, J=7.5 Hz, Et), 6.94 (d, 2H, J=8.4 Hz, Ar-H), 7.58 (dd, 2H, J=8.0, 7.2 Hz, Ar-H), 7.71 (t, 1H, J=8.0 Hz, Ar-H), 7.75 (t, 1H, J=8.4 Hz, Ar-H), 7.99 (d, 2H, J=7.2 Hz, Ar-H), 9.68 (s, 1H, *meso*-H), 9.77 (s, 1H, *meso*-H). HRMS (FAB): Found: m/z 824.361. Calcd for $C_{50}H_{56}O_3N_4Zn$: M^+, 824.364. IR (KBr) ν_{max} 1711 cm^{-1} (CO).

10. Mp >300 °C. ^{1}H NMR ($CDCl_3$) δ=−1.69 (s, 1H, NH), −0.82 (broad, 1H, NH), 0.26 (t, 6H, J=7.3 Hz, rearranged-Et), 1.13 (t, 3H, J=7.4 Hz, Et), 1.16 (t, 3H, J=7.6 Hz, Et), 1.19 (t, 3H, J=7.4 Hz, Et), 1.77 (t, 3H, J=7.3 Hz, Et), 1.80 (t, 3H, J=7.7 Hz, Et), 1.85 (t, 3H, J=7.8 Hz, Et), 2.17 (m, 4H, J=7.3 Hz, rearranged-Et), 2.67 (q, 2H, J=7.4 Hz, Et), 2.87 (q, 2H, J=7.6 Hz, Et), 3.03 (q, 2H, J=7.4 Hz, Et), 3.55 (s, 6H, OMe), 3.84 (q, 2H, J=7.3 Hz, Et), 3.99 (q, 2H, J=7.7 Hz, Et), 4.00 (q, 2H, J=7.8 Hz, Et), 6.94 (d, 2H, J=8.4 Hz, Ar-H), 7.64 (dd, 2H, J=8.0, 7.5 Hz, Ar-H), 7.75 (t, 1H, J=8.0 Hz, Ar-H), 7.75 (t, 1H, J=8.4 Hz, Ar-H), 8.03 (d, 2H, J=7.5 Hz, Ar-H), 9.95 (s, 1H, *meso*-H), 10.00 (s, 1H, *meso*-H). HRMS (FAB): Found: m/z 763.453. Calcd for $C_{50}H_{59}O_3N_4$: M^++H, 763.459. IR (KBr) ν_{max} 1714 cm^{-1} (CO).

Synthesis of Porphyrin–Oxochlorin Heterodimers. The synthesis of **1**—**3** was described in detail. A solution of the di-(2-pyrrolyl)methane **19**[42] (135 mg, 0.588 mmol) in 10 ml of acetonitrile was added to a solution of *p*-tolualdehyde (67 mg, 0.56 mmol), **17** (30 mg, 28.0 μmol) and trichloroacetic acid (100 mg, 0.61 mmol) in acetonitrile (10 ml). The resulting solution was stirred for 6 h at room temperature under an Ar atmosphere in the dark. A solution of *p*-chloranil (217 mg, 0.882 mmol) in THF (30 ml) was added and the reaction mixture was stirred for an additional 1 h. After evaporation of the solvent, the residue was dissolved in CH_2Cl_2 (50 ml) and the resulting solution was washed with 4 M HCl (90 ml) and with aqueous Na_2CO_3 (200 ml), and dried over anhydrous Na_2SO_4. After metalation with $Zn(OAc)_2$, the bis-zinc heterodimer **1** was separated by flash column chromatography on silica gel (CH_2Cl_2/Et_2O (98/2) eluent; begin eluted as a dark violet band) and was recrystallized from CH_2Cl_2/hexane, (26 mg, 0.15 μmol, 52% yield based on the amount of **15** used). The free-base heterodimer **3** was prepared by usual demetalation of **1** with 3 M HCl solution in almost quantitative yield, and the hybrid heterodimer **2** was prepared by the selective metalation of the P moiety of **3** with an equimolar amount of $Zn(OAc)_2$ at 0 °C in CH_2Cl_2. The progress of the metalation was monitored by thin-layer chromatography. After the metalation was complete at the porphyrin moiety, **2** was separated by silica gel flash column chromatography in 70% yield.

1. Mp >300 °C. ^{1}H NMR ($CDCl_3$) δ=0.31 (t, 6H, J=7.3 Hz, rearranged-Et), 0.91 (t, 3 Hz, Hexyl-Me), 1.03 (t, 3H, J=7.6 Hz, Et), 1.34 (t, 6H, J=7.4 Hz, Et), 1.34 (m, 6H, Hexyl-CH_2), 1.74 (m, 2H, Hexyl-CH_2), 1.79 (t, 3H, J=7.6 Hz, Et), 1.82 (t, 3H, J=7.6 Hz, Et), 1.82 (t, 3H, J=7.6 Hz, Et), 1.83 (t, 3H, J=7.5 Hz, Et), 1.85 (t, 3H, J=7.5 Hz, Et), 1.91 (t, 6H, J=7.5 Hz, Et), 2.12 (m, 4H, J=7.3 Hz, rearranged-Et), 2.34 (q, 2H, J=7.6 Hz, Et), 2.52 (s, 6H, Me), 2.76 (s, 3H, Tolyl-Me), 3.40 (s, 6H, Me), 3.65 (q, 2H, J=7.4 Hz, Et), 3.66 (q, 2H, J=7.4 Hz, Et), 3.73 (s, 6H, OMe), 3.79 (t, 2H, Hexyl-CH_2), 3.82 (q, 2H, J=7.6 Hz, Et), 3.95 (q, 2H, J=7.6 Hz, Et), 3.96 (q, 2H, J=7.6 Hz, Et), 4.05 (q, 4H, J=7.5 Hz, Et), 4.18 (q, 4H, J=7.5 Hz, Et), 5.22 (s, 2H, Benzyl-CH_2), 7.58 (d, 2H, J=7.9 Hz, Ar-H), 7.65 (d, 2H, J=7.9 Hz, Ar-H), 7.86 (s, 2H, Ar-H), 7.98 (d, 2H, J=7.9 Hz, Ar-H), 7.99 (d, 2H, J=7.9 Hz, Ar-H), 8.41 (s, 2H, Im–Ar-H), 9.71 (s, 1H, *meso*-H), 9.82 (s, 1H, *meso*-H), 10.27 (s, 2H, *meso*-H). HRMS (FAB): Found: m/z 1764.728. Calcd for $C_{106}H_{112}O_7N_{10}Zn_2$: M^+, 1764.730. IR (KBr) ν_{max} 1718 cm^{-1} (CO, CHO, imide CO).

2. Mp 298—300 °C. ^{1}H NMR ($CDCl_3$) δ=−1.34 (s, 1H, NH), −0.25 (broad, 1H, NH), 0.29 (t, 6H, J=7.2 Hz, rearranged-Et), 0.91 (t, 3H, Hexyl-Me), 1.13 (t, 3H, J=7.7 Hz, Et), 1.36 (m, 6H, Hexyl-CH_2), 1.45 (t, 3H, J=7.6 Hz, Et), 1.51 (t, 3H, J=7.3 Hz, Et), 1.74 (m, 2H, Hexyl-CH_2), 1.82 (t, 6H, J=7.8 Hz, Et), 1.87 (t, 6H, J=7.9 Hz, Et), 1.91 (t, 6H, J=8.1 Hz, Et), 1.93 (t, 3H, J=8.0 Hz, Et), 2.17 (m, 4H, J=7.2 Hz, rearranged-Et), 2.53 (s, 6H, Me), 2.62 (q, 2H, J=7.7 Hz, Et), 2.76 (s, 3H, Tolyl-Me), 3.40 (s, 3H, Me), 3.42 (s, 3H, Me), 3.67 (q, 2H, J=7.6 Hz, Et), 3.70 (s, 6H, OMe), 3.79 (t, 2H, Hexyl-CH_2), 3.83 (q, 2H, J=7.3 Hz, Et), 4.01 (q, 4H, J=7.9 Hz, Et), 4.06 (q, 4H, J=7.8 Hz, Et), 4.15 (q, 2H, J=8.0 Hz, Et), 4.20 (q, 4H, J=8.1 Hz, Et), 5.24 (s, 2H, Benzyl-CH_2), 7.58 (d, 2H, J=8.0 Hz, Ar-H), 7.70 (d, 2H, J=8.0 Hz, Ar-H), 7.86 (s, 2H, Ar-H), 7.98 (d, 2H, J=8.0 Hz, Ar-H), 8.03 (d, 2H, J=8.0 Hz, Ar-H), 8.41 (s, 2H, Im–Ar-H), 10.02 (s, 1H, *meso*-H), 10.09 (s, 1H,

meso-H), 10.29 (s, 2H, *meso*-H). HRMS (FAB): Found: m/z 1703.820. Calcd for $C_{106}H_{115}O_7N_{10}Zn$: $M^+ + H$, 1703.824. IR (KBr) ν_{max} 1720 cm^{-1} (CO, imide CO).

3. Mp >300 °C. ^1H NMR ($CDCl_3$) $\delta = -2.04$ (broad, 1H, NH), −1.88 (broad, 1H, NH), −1.39 (s, 1H, NH), −0.31 (broad, 1H, NH), 0.29 (t, 6H, J=7.5 Hz, rearranged-Et), 0.91 (t, 3H, Hexyl-Me), 1.13 (t, 3H, J=7.8 Hz, Et), 1.35 (m, 6H, Hexyl-CH_2), 1.45 (t, 3H, J=7.6 Hz, Et), 1.51 (t, 3H, J=7.5 Hz, Et), 1.73 (m, 2H, Hexyl-CH_2), 1.83 (t, 6H, J=7.7 Hz, Et), 1.87 (t, 3H, J=7.6 Hz, Et), 1.88 (t, 3H, J=7.6 Hz, Et), 1.92 (t, 6H, J=7.6 Hz, Et), 1.93 (t, 3H, J=7.5 Hz, Et), 2.17 (m, 4H, J=7.5 Hz, rearranged-Et), 2.56 (s, 6H, Me), 2.61 (q, 2H, J=7.8 Hz, Et), 2.75 (s, 3H, Tolyl-Me), 3.40 (s, 3H, Me), 3.43 (s, 3H, Me), 3.62 (q, 2H, J=7.6 Hz, Et), 3.70 (s, 6H, OMe), 3.78 (t, 2H, Hexyl-CH_2), 3.79 (q, 2H, J=7.5 Hz, Et), 4.01 (q, 4H, J=7.7 Hz, Et), 4.08 (q, 4H, J=7.6 Hz, Et), 4.15 (q, 2H, J=7.5 Hz, Et), 4.22 (q, 4H, J=7.6 Hz, Et), 5.23 (s, 2H, Benzyl-CH_2), 7.58 (d, 2H, J=8.0 Hz, Ar-H), 7.69 (d, 2H, J=8.0 Hz, Ar-H), 7.84 (s, 2H, Ar-H), 7.97 (d, 2H, J=8.0 Hz, Ar-H), 8.03 (d, 2H, J=8.0 Hz, Ar-H), 8.36 (s, 2H, Im–Ar-H), 10.03 (s, 1H, *meso*-H), 10.09 (s, 1H, *meso*-H), 10.35 (s, 2H, *meso*-H). HRMS (FAB): Found: m/z 1641.906. Calcd for $C_{106}H_{117}O_7N_{10}$: $M^+ + H$, 1641.911. IR (KBr) ν_{max} 1720 cm^{-1} (CO, imide CO).

The heterodimer **4** was prepared from *p*-tolualdehyde, **19**, and **22** in 48% yield essentially in the same manner as described for **1**, and was converted into **6** and then to **5** in almost quantitative yields.

4. Mp >300 °C. ^1H NMR ($CDCl_3$) $\delta = 0.33$ (t, 6H, J=7.4 Hz, rearranged-Et), 1.13 (t, 3H, J=7.4 Hz, Et), 1.34 (t, 3H, J=7.3 Hz, Et), 1.35 (t, 3H, J=7.6 Hz, Et), 1.82 (t, 3H, J=7.7 Hz, Et), 1.82 (t, 6H, J=7.8 Hz, Et), 1.86 (t, 3H, J=7.6 Hz, Et), 1.88 (t, 3H, J=7.6 Hz, Et), 1.90 (t, 6H, J=7.5 Hz, Et), 2.20 (m, 4H, J=7.4 Hz, rearranged-Et), 2.48 (q, 2H, J=7.4 Hz, Et), 2.52 (s, 6H, Me), 2.68 (s, 3H, Tolyl-Me), 2.76 (s, 3H, Tolyl-Me), 3.40 (s, 6H, Me), 3.66 (q, 2H, J=7.3 Hz, Et), 3.67 (q, 2H, J=7.6 Hz, Et), 3.73 (s, 6H, OMe), 3.86 (q, 2H, J=7.7 Hz, Et), 3.96 (q, 2H, J=7.8 Hz, Et), 3.97 (q, 2H, J=7.8 Hz, Et), 4.05 (q, 4H, J=7.6 Hz, Et), 4.19 (q, 4H, J=7.5 Hz, Et), 7.42 (d, 2H, J=8.0 Hz, Ar-H), 7.58 (d, 2H, J=7.9 Hz, Ar-H), 7.86 (s, 2H, Ar-H), 7.89 (d, 2H, J=8.0 Hz, Ar-H), 7.98 (d, 2H, J=7.9 Hz, Ar-H), 9.72 (s, 1H, *meso*-H), 9.83 (s, 1H, *meso*-H), 10.28 (s, 2H, *meso*-H). HRMS (FAB): Found: m/z 1466.632. Calcd for $C_{90}H_{98}O_3N_8Zn_2$: M^+, 1466.635. IR (KBr) ν_{max} 1709 cm^{-1} (CO).

5. Mp 297—298 °C. ^1H NMR ($CDCl_3$) $\delta = -1.33$ (s, 1H, NH), −0.23 (broad, 1H, NH), 0.31 (t, 6H, J=7.3 Hz, rearranged-Et), 1.23 (t, 3H, J=7.2 Hz, Et), 1.46 (t, 3H, J=7.7 Hz, Et), 1.52 (t, 3H, J=7.4 Hz, Et), 1.82 (t, 6H, J=7.6 Hz, Et), 1.88 (t, 3H, J=7.4 Hz, Et), 1.90 (t, 3H, J=7.1 Hz, Et), 1.92 (t, 6H, J=7.4 Hz, Et), 1.94 (t, 3H, J=7.5 Hz, Et), 2.22 (m, 4H, J=7.3 Hz, rearranged-Et), 2.53 (s, 6H, Me), 2.70 (s, 3H, Tolyl-Me), 2.76 (s, 3H, Tolyl-Me), 2.76 (q, 2H, J=7.2 Hz, Et), 3.40 (s, 3H, Me), 3.43 (s, 3H, Me), 3.68 (q, 2H, J=7.7 Hz, Et), 3.70 (s, 6H, OMe), 3.84 (q, 2H, J=7.4 Hz, Et), 4.02 (q, 4H, J=7.6 Hz, Et), 4.05 (q, 2H, J=7.4 Hz, Et), 4.07 (q, 2H, J=7.1 Hz, Et), 4.16 (q, 2H, J=7.5 Hz, Et), 4.20 (q, 4H, J=7.4 Hz, Et), 7.47 (d, 2H, J=7.3 Hz, Ar-H), 7.58 (d, 2H, J=7.3 Hz, Ar-H), 7.86 (s, 2H, Ar-H), 7.93 (d, 2H, J=7.3 Hz, Ar-H), 7.98 (d, 2H, J=7.3 Hz, Ar-H), 10.03 (s, 1H, *meso*-H), 10.10 (s, 1H, *meso*-H), 10.29 (s, 2H, *meso*-H) HRMS (FAB): Found: m/z 1405.730. Calcd for $C_{90}H_{101}O_3N_8Zn$: $M^+ + H$, 1405.729. IR (KBr) ν_{max} 1711 cm^{-1} (CO).

6. Mp >300 °C. ^1H NMR ($CDCl_3$) $\delta = -1.92$ (broad, 1H, NH, the other NH was not detected), −1.38 (s, 1H, NH), −0.30 (broad, 1H, NH), 0.31 (t, 6H, J=7.2 Hz, rearranged-Et), 1.23 (t, 3H, J=7.4 Hz, Et), 1.46 (t, 3H, J=7.4 Hz, Et), 1.51 (t, 3H, J=7.6 Hz, Et), 1.83 (t, 6H, J=7.6 Hz, Et), 1.89 (t, 3H, J=7.7 Hz, Et), 1.91 (t, 3H, J=7.8 Hz, Et), 1.92 (t, 6H, J=7.9 Hz, Et), 1.94 (t, 3H, J=7.9 Hz, Et), 2.23 (m, 4H, J=7.2 Hz, rearranged-Et), 2.56 (s, 6H, Me), 2.69 (s, 3H, Tolyl-Me), 2.75 (s, 3H, Tolyl-Me), 2.76 (q, 2H, J=7.4 Hz, Et), 3.41 (s, 3H, Me), 3.43 (s, 3H, Me), 3.62 (q, 2H, J=7.4 Hz, Et), 3.70 (s, 6H, OMe), 3.79 (q, 2H, J=7.6 Hz, Et), 4.02 (q, 4H, J=7.6 Hz, Et), 4.05 (q, 2H, J=7.7 Hz, Et), 4.08 (q, 2H, J=7.8 Hz, Et), 4.16 (q, 2H, J=7.9 Hz, Et), 4.22 (q, 4H, J=7.9 Hz, Et), 7.47 (d, 2H, J=7.9 Hz, Ar-H), 7.58 (d, 2H, J=8.0 Hz, Ar-H), 7.84 (s, 2H, Ar-H), 7.93 (d, 2H, J=7.9 Hz, Ar-H), 7.97 (d, 2H, J=8.0 Hz, Ar-H), 10.04 (s, 1H, *meso*-H), 10.10 (s, 1H, *meso*-H), 10.35 (s, 2H, *meso*-H). HRMS (FAB): Found: m/z 1343.800. Calcd for $C_{90}H_{103}O_3N_8$: $M^+ + H$, 1343.815. IR (KBr) ν_{max} 1712 cm^{-1} (CO, CHO).

We thank Professor T. Ohno and Dr. K. Nozaki of Osaka University for the measurement of nanosecond transient absorption spectra. This work was partially supported by a Grant-in-Aid for Specially Promoted Research No. 02102005 from the Ministry of Education, Science and Culture.

References

1) J. Deisenhofer, O. Epp, K. Miki, R. Huber, and H. Michel, *Nature*, **318**, 618 (1985).

2) C. Kirmaier and D. Holten, *Photosynth. Res.*, **13**, 225 (1987).

3) W. Holtzapfel, U. Finkele, W. Kaiser, D. Oesterhelt, H. Scheer, H. U. Stilz, and W. Zinth, *Chem. Phys. Lett.*, **160**, 1 (1989).

4) M. R. Wasielewski, *Chem. Rev.*, **92**, 435 (1992); D. Gust and T. A. Moore, *Science*, **244**, 35 (1989); K. Maruyama and A. Osuka, *Pure Appl. Chem.*, **62**, 1511 (1990); A. M. Brun, A. Harriman, V. Heitz, and J. P. Savauge, *J. Am. Chem. Soc.*, **113**, 8657 (1991); D. Heiler, G. McLendon, and P. Rogalskyj, *J. Am. Chem. Soc.*, **109**, 604 (1987); J. L. Sessler, V. L. Capuano, and A. Harriman, *J. Am. Chem. Soc.*, **115**, 4618 (1993); E. J. Atkins, A. M. Oliver, and M. N. Paddon-Row, *Tetrahedron Lett.*, **34**, 6147 (1993); F. Pollinger, H. Heitele, M. E. Michel-Beyerle, M. Tercel, and H. A. Staab, *Chem. Phys. Lett.*, **209**, 251 (1993); J. M. Zaleski, C. K. Chang, G. E. Leroi, R. I. Cukier, and D. G. Nocera, *J. Am. Chem. Soc.*, **114**, 3564 (1992).

5) J. R. Darwent, P. Douglas, A. Harriman, G. Porter, and M. -C. Richoux, *Coord. Chem. Rev.*, **44**, 83 (1982).

6) D. Gust, T. A. Moore, A. L. Moore, A. N. Macpherson, A. Lopez, J. M. DeGraziano, I. Gouni, E. Bittersman, G. R. Seely, R. A. Nieman, X. C. Ma, L. J. Demanche, S. C. Hung, D. K. Luttrull, S. J. Lee, and P. K. Kerrigan, *J. Am. Chem. Soc.*, **115**, 11141 (1993).

7) M. R. Wasielewski, M. P. Niemczyk, W. A. Svec, and

E. B. Pewitt, *J. Am. Chem. Soc.*, **107**, 5562 (1985); M. R. Wasielewski, G. L. Gaines, III, M. P. O'Neil, W. A. Svec, and M. P. Niemczyk, *J. Am. Chem. Soc.*, **112**, 4559 (1990).

8) A. Osuka, T. Nagata, F. Kobayashi, R. P. Zhang, K. Maruyama, N. Mataga, T. Asahi, T. Ohno, and K. Nozaki, *Chem. Phys. Lett.*, **199**, 302 (1992); A. Osuka, R. P. Zhang, K. Maruyama, T. Ohno, and K. Nozaki, *Chem. Lett.*, **1993**, 1727; A. Osuka, R. P. Zhang, K. Maruyama, T. Ohno, and K. Nozaki, *Bull. Chem. Soc. Jpn.*, **66**, 3773 (1993); A. Osuka, R. P. Zhang, K. Maruyama, N. Mataga, Y. Tanaka, and T. Okada, *Chem. Phys. Lett.*, **215**, 179 (1993).

9) A. Osuka, S. Nakajima, K. Maruyama, N. Mataga, T. Asahi, I. Yamazaki, Y. Nishimura, T. Ohno, and K. Nozaki, *J. Am. Chem. Soc.*, **115**, 4577 (1993).

10) S. Nishitani, N. Kurata, Y. Sakata, S. Misumi, A. Karen, T. Okada, and N. Mataga, *J. Am. Chem. Soc.*, **105**, 7771 (1983).

11) N. Mataga, A. Karen, T. Okada, S. Nishitani, N. Kurata, Y. Sakata, and S. Misumi, *J. Phys. Chem.*, **88**, 5138 (1984).

12) M. Ohkohchi, A. Takahashi, N. Mataga, T. Okada, A. Osuka, H. Yamada, and K. Maruyama, *J. Am. Chem. Soc.*, **115**, 12137 (1993).

13) Gust and Moore reported a carotenoid–diporphyrin triads in which intramolecular CS within the diporphyrin moiety is followed by a hole transfer to the carotenoid: D. Gust, T. A. Moore, A. L. Moore, F. Gao, D. Luttrull, J. M. DeGraziano, X. C. Ma, L. R. Makings, S. J. Lee, T. T. Trier, E. Bitteresmann, G. R. Seely, S. Woodward, R. V. Bensasson, M. Rougee, F. C. De Schryver, and M. Van der Auweraer, *J. Am. Chem. Soc.*, **113**, 3638 (1991).

14) N. Nakashima, M. Murakawa, and N. Mataga, *Bull. Chem. Soc. Jpn.*, **91**, 4490 (1976).

15) N. Mataga, H. Yao, T. Okada, and W. Rettig, *J. Phys. Chem.*, **93**, 3383 (1989); T. Okada, S. Nishikawa, K. Kanaji, and N. Mataga, "Ultrafast Phenomena VII," ed by C. B. Harris et al., Springer, Berlin (1990), p. 397; N. Mataga, *Pure Appl. Chem.*, **65**, 1605 (1993).

16) N. Mataga, H. Yao, and T. Okada, *Tetrahedron*, **45**, 4683 (1989); T. Hayashi, N. Suzuki, N. Mataga, Y. Sakata, and S. Misumi, *J. Phys. Chem.*, **81**, 420 (1977); H. Yao, T. Okada, and N. Mataga, *J. Phys. Chem.*, **93**, 7388 (1989).

17) M. R. Wasielewski, D. G. Johnson, M. P. Niemczyk, G. L. Gaines, III, M. P. O'Neil, and W. A. Svec, *J. Am. Chem. Soc.*, **112**, 6482 (1990).

18) D. G. Johnson, M. P. Niemczyk, D. W. Minsek, G. P. Wiederrecht, W. A. Svec, G. L. Gaines, III, and M. R. Wasielewski, *J. Am. Chem. Soc.*, **115**, 5692 (1993); G. P. Wiederrecht, S. Watanabe, and M. R. Wasielewski, *Chem. Phys.*, **176**, 601 (1993).

19) M. R. Wasielweski, G. L. Gaines, III, G. P. Wiederrecht, W. A. Svec, and M. P. Niemczyk, *J. Am. Chem. Soc.*, **115**, 10442 (1993).

20) H. Fisher and H. Orth, in "Die Chemie des Pyrrols," Akademische Verlag, Leipzig, Germany (1937), Vol. 2, Part 1, p. 269; H. Fisher and H. Pfeiffer, *Justus Liebigs Ann. Chem.*, **556**, 131 (1944).

21) H. Inhoffen and W. Notle, *Justus Liebigs Ann. Chem.*, **725**, 167 (1969).

22) C. K. Chang and C. Sotiriou, *J. Org. Chem.*, **50**, 4989 (1985).

23) R. Bonnett, M. J. Dimsdale, and G. F. Stephenson, *J. Chem. Soc. C*, **1969**, 564.

24) A. M. Stolzenberg, P. A. Glazer, and B. M. Foxman, *Inorg. Chem.*, **25**, 983 (1986).

25) R. K. Pandey, F. -Y. Shiau, M. Isaac, S. Ramaprasad, T. J. Dougherty, and K. M. Smith, *Tetrahedron Lett.*, **33**, 7815 (1992).

26) A. Osuka, S. Marumo, and K. Maruyama, *Bull. Chem. Soc. Jpn.*, **66**, 3837 (1993).

27) A. Osuka, T. Nagata, F. Kobayashi, and K. Maruyama, *J. Heterocycl. Chem.*, **27**, 1657 (1990); T. Nagata, A. Osuka, and K. Maruyama, *J. Am. Chem. Soc.*, **112**, 3054 (1990).

28) It is interesting to note that the electronic interactions in an orthogonal porphyrin–pyropheophorbide dyad results in blue shift in the pyropheophorbide Qy-bands (Ref. 17) in the opposite direction observed here.

29) A. Weller, *Z. Phys. Chem. (Wiesbaden)*, **133**, 93 (1982).

30) N. Mataga, A. Karen, T. Okada, S. Nishitani, N. Kurata, Y. Sakata, and S. Misumi, *J. Am. Chem. Soc.*, **106**, 2442 (1984); N. Mataga, A. Karen, T. Okada, S. Nishitani, Y. Sakata, and S. Misumi, *J. Phys. Chem.*, **88**, 4650 (1984).

31) T. Asahi, M. Ohkohchi, R. Matsusaka, N. Mataga, R. P. Zhang, A. Osuka, and K. Maruyama, *J. Am. Chem. Soc.*, **115**, 5665 (1993).

32) J. M. Warman, K. J. Smit, S. A. Jonker, J. W. Verhoeven, H. Oevering, J. Kroon, M. N. Paddon-Row, and A. M. Oliver, *Chem. Phys.*, **170**, 359 (1993); Y. Zeng and M. B. Zimmt, *J. Phys. Chem.*, **96**, 8395 (1992); G. L. Closs and J. R. Miller, *Science*, **240**, 440 (1988); G. L. Gaines, III, M. P. O'Neil, W. A. Svec, M. P. Niemczyk, and M. R. Wasielewski, *J. Am. Chem. Soc.*, **113**, 719 (1991).

33) Singlet-singlet energy transfer is common to covalently linked porphyrin–chlorin dyads. Refs. 17, 18, and 19, Ref. 35; D. Gust, T. A. Moore, A. N. Moore, A. A. Krasnovky, Jr., P. A. Liddell, D. Nicodem, J. M. DeGraziano, P. Kerrigan, L. R. Makings, and P. J. Pessiki, *J. Am. Chem. Soc.*, **115**, 5684 (1993); M. Raghavan and V. Krishnan, *Chem. Phys. Lett.*, **205**, 19 (1993).

34) N. Mataga, T. Asahi, Y. Kanda, T. Okada, and T. Kakitani, *Chem. Phys.*, **127**, 249 (1988); T. Asahi and N. Mataga, *J. Phys. Chem.*, **93**, 6575 (1989).

35) D. Gust, T. A. Moore, A. N. Moore, L. Leggett, S. Lin, J. M. DeGraziano, R. M. Hermant, D. Nicodem, P. Craig, G. R. Seely, and R. A. Nieman, *J. Phys. Chem.*, **97**, 7926 (1993).

36) I. Yamazaki, N. Tamai, H. Kume, H. Tsuchiya, and K. Oba, *Rev. Sci. Instrum.*, **56**, 1187 (1985).

37) H. Miyasaka, H. Masuhara, and N. Mataga, *Laser Chem.*, **1**, 357 (1983).

38) Y. Hirata and N. Mataga, *J. Phys. Chem.*, **95**, 1640 (1991).

39) T. Ohno, A. Yoshimura, and N. Mataga, *J. Phys. Chem.*, **94**, 4871 (1990).

40) N. Ono, H. Kawamura, M. Bougauchi, and K. Maruyama, *Tetrahedron*, **46**, 7483 (1990).

41) T. Nagata, *Bull. Chem. Soc. Jpn.*, **64**, 3005 (1991).

42) P. S. Clezy and A. W. Nichol, *Aust. J. Chem.*, **11**, 1835 (1965). This di-(2-prrolyl)methane was more conveniently prepared in a large scale by the isonitrile route, Ref. 40.